Biomaterials Science

ROYAL SOCIETY OF CHEMISTRY

PAPER

View Article Online
View Journal | View Issue

Cite this: *Biomater. Sci.*, 2020, **8**, 3147

ZBTB20-mediated titanium particle-induced peri-implant osteolysis by promoting macrophage inflammatory responses†

Junxiong Qiu,‡[a,b] Peng Peng,‡[a] Min Xin,‡[c] Zhenkang Wen,[a] Zhong Chen,[a] Sipeng Lin,[a] Manyuan Kuang,[a] Yuan Fu,[a] Guibin Fang,[a] Shixun Li,[a] Changchuan Li,[a] Jiaji Mao,[d] Ling Qin*[e] and Yue Ding *[a]

Aseptic loosening (AL) caused by wear particles released from implant surfaces is one of the main causes for the failure of artificial joints, which is initiated by macrophage inflammatory responses. Emerging evidence suggests that the member of a broad-complex, tramtrack, bric-a-brac/poxvirus and zinc finger (BTB/POZ) family as well as zinc finger and BTB domain-containing protein 20 (ZBTB20) can inhibit IκBα gene transcription, promote NF-κB activation, and initiate innate immune responses. The molecular mechanism(s) by which ZBTB20 contributes to titanium particle (TiP)-induced macrophage inflammatory responses and osteolysis has not been fully elucidated. Here, we showed that ZBTB20 increased either in the AL group's synovial membranes or in TiP-stimulated bone-marrow-derived macrophages (BMDMs) as compared to that in the control groups. Moreover, the knockdown of ZBTB20 led to the inhibition of proinflammatory factors induced by TiPs in BMDMs, such as tumor necrosis factor-α (TNF-α), interleukin-6 (IL-6), and interferon-β (IFN-β). Here, we also reported that the knockdown of ZBTB20 suppressed TiP-induced NF-κB activation and M1 polarization as well as stabilized the trans Golgi network (TGN) in BMDMs. The dual-luciferase reporter assay identified the binding between the IκBα promoter and ZBTB20, and IκBα knockdown could rescue the antiinflammatory effects induced by the ZBTB20 knockdown in BMDMs. Finally, we found that sh-ZBTB20 lentivirus injection could reduce TiP-induced osteolysis in mouse calvaria, inhibiting TiP-induced proinflammatory factors and loss of bone volume/total volume (BV/TV) as well as bone mineral density (BMD). These results suggest that ZBTB20 positively regulated NF-κB activation and M1 polarization as well as the production of TGN-derived tubular carriers in BMDMs, playing a positive role in macrophage activation and mouse cranial osteolysis induced by TiPs. It may be a potential therapeutic target for the prevention of aseptic loosening of prostheses.

Received 24th January 2020,
Accepted 15th March 2020

DOI: 10.1039/d0bm00147c

rsc.li/biomaterials-science

1. Introduction

A higher rate of age-related joint diseases has been documented in the aging population, and arthroplasty has become the most effective treatment methodology for such severe joint diseases. Although considerable efforts have been made toward improving the efficacy of prosthesis,[1] revision surgeries still persist in almost 7% patients within 10 years after undergoing primary arthroplasty, and particle-induced periprosthetic osteolysis and subsequent aseptic loosening (AL) are some of the main causes for performing revision surgeries.[2] A number of studies have shown that the wear particles released from the surfaces of implants, which can be phagocytized by macrophages and incite an adverse immunoreaction, play a critical role in osteolysis.[3] Macrophages secrete proinflammatory cytokines, such as tumor necrosis factor alpha (TNF-α) and interleukin-6 (IL-6),[4] which increase osteoclastic bone resorption

[a]*Department of Orthopaedic Surgery, Sun Yat-sen Memorial Hospital, Sun Yat-sen University, Guangzhou 510120, China. E-mail: dingyue@mail.sysu.edu.cn*
[b]*Guangdong Provincial Key Laboratory of Malignant Tumor Epigenetics and Gene Regulation, Sun Yat-sen Memorial Hospital, Sun Yat-sen University, Guangzhou 510120, China*
[c]*Zhongshan School of Medicine, Sun Yat-sen University, Guangzhou 510000, China*
[d]*Department of Radiology, Sun Yat-sen Memorial Hospital, Sun Yat-sen University, Guangzhou 510120, China*
[e]*Musculoskeletal Research Laboratory Department of Orthopaedics & Taumatology and Innovative Orthopaedic Biomaterial and Drug Translational Research Laboratory of Li Ka Shing Institute of Health Sciences, the Chinese University of Hong Kong, SAR, PR China. E-mail: lingqin@cuhk.edu.hk*

†Electronic supplementary information (ESI) available. See DOI: 10.1039/d0bm00147c

‡These authors contributed equally to this work.

and reduce osteoblastic bone formation. Consequently, it is highly desirable to find a method to suppress macrophages' proinflammatory functions to prolong the lifespan of prosthesis.

Emerging evidence suggests that ZBTB20 plays an important role in multiple systems, and it has been reported that mice lacking ZBTB20 exhibit severe phenotypes such as growth retardation, premature lethality, infertility, and hypoglycemia.[5] ZBTB20, also known as dendritic cell-derived broad-complex, tramtrack, bric-a-brac/poxvirus and zinc finger (BTB/POZ) zinc finger (DPZF), belongs to a subfamily of zinc finger proteins containing Cys2-His2 (C2H2) Krüppel-like zinc fingers and BTB/POZ domains; furthermore, it primarily functions as a transcriptional repressor.[6] Moreover, ZBTB20 contains five C2H2 zinc fingers at the C terminal and a BTB domain at the N terminal; further, C2H2 zinc fingers can bind to promoters, while the BTB domain functions in protein–protein interactions.[7] In a recent study, ZBTB20 was demonstrated to inhibit *IκBα* gene transcription, promoting NF-κB activation; further, the knockout of ZBTB20 in myeloid cells protected mice from endotoxin shock and *Escherichia coli*–caused sepsis.[8]

Some studies, including ours, have proven that the NF-κB pathway plays a key role in titanium particles (TiPs)-induced macrophage activation, which partly contributes toward periprosthetic osteolysis and AL.[9,10] Moreover, studies have suggested that ZBTB20 could play a key role in the NF-κB pathway, as well as the activation and polarization of macrophages.[8,11] However, the molecular mechanism(s) by which ZBTB20 contributes toward TiPs-induced macrophage activation, resulting in periprosthetic osteolysis and AL, is not fully understood. In this study, we demonstrated that the knockdown of ZBTB20 reduced the TiPs-induced proinflammatory factors produced by macrophages, potentially by the downregulation of the NF-κB pathway and stabilizing the trans Golgi network (TGN), resulting in decreased M1 polarization and increased M2 polarization. Most interestingly, we found that TiPs-induced osteolysis in mouse calvaria could be attenuated by sh-ZBTB20 lentivirus injection.

2. Materials and methods

2.1 Clinical specimen collection, immunohistochemistry (IHC) assay, and histological analysis

The clinical specimens of the synovial membranes were acquired from 7 patients at the Department of Orthopaedic Surgery, Sun Yat-sen Memorial Hospital, Sun Yat-sen University (3 males and 4 females; average age: 59.4 ± 4.0 years; average duration after primary total hip arthroplasty (THA): 16.35 ± 2.8 years), who underwent prosthesis revision surgery on account of AL, as well as that from 8 patients (3 males and 5 females; average age: 66.6 ± 14.6 years) who had primary THA on account of femoral head necrosis (FHN). In the AL group, the specimens had synovial membranes around the prosthesis; in the FHN group, the specimens had hip synovial membranes. All the experiments were performed in accordance with the established guidelines for human care, and experiments were approved by the ethics committee at the Sun Yat-sen University, Sun Yat-sen Memorial Hospital (2017 ethic record no.: 26). Informed consents were obtained from the human participants of this study.

Clinical specimens were put in 4% paraformaldehyde (PFA) for 12 h and then transparentized by xylene for 20 min and embedded in 54 °C paraffin for sectioning. Here, C57BL/6J male mouse calvaria were decalcified in an ethylenediaminetetraacetic acid (EDTA) decalcifying solution (E1171, Solarbio) for 21 days. Thereafter, the samples were fixed in 4% PFA for 12 h and then embedded in 54 °C paraffin blocks for sectioning.

For the IHC assay, the sections were heated at 60 °C for 2 h and then put in xylene for 20 min and sequentially dehydrated with 100% ethanol, 95% ethanol, and 75% ethanol for 5 min, followed by washing in phosphate-buffered saline (PBS) (GNM20012, Genom) 3 times. Then, 0.1% Triton X-100 (9002-93-1, Sigma-Aldrich) was dropped on the sections at 20 °C for 20 min, followed by washing with PBS 3 times. Antigen retrieval was performed with pepsin (ZLI-9013, ZSGB-BIO) at 37 °C for 20 min, followed by washing with PBS 3 times. Five percent bovine serum albumin (BSA) (CCS30014.01, Molecular Research Center, Inc.) was used as a blocking buffer at 37 °C for 30 min; then, diluted primary antibodies were added on the sections at 37 °C for 2 h followed by washing with PBS 3 times. TNF-α antibody (rabbit, A11543, Abclonal), IL-6 antibody (rabbit, 21865-1-AP, Proteintech), and ZBTB20 antibody (rabbit, NBP2-20936, Novus Biologicals) were used as the primary antibodies. Secondary antibodies labelled with horseradish peroxidase (HRP) (goat anti-rabbit, ab6721, Abcam) were used at 37 °C for 30 min followed by washing with PBS 3 times. A DAB HRP color development kit (P0203, Beyotime Biotechnology) was used for detection for 5 min, followed by washing with flowing water for 5 min. Hematoxylin was used for nuclear staining for 20 s, followed by washing under flowing tap water for 10 min and drying. Neutral balsam was used for mount preparation, and a biomicroscope (DM2000, Leica) was used for observation. Ten views of each immunostained section were independently evaluated by two expert pathologists in a blind fashion. Bresalier's semiquantitative scoring system was used, which determined both staining intensity (0 for no stain; 1 for weak stain; 2 for moderate stain; 3 for strong stain) and the percentage of stained cells. The scores of staining intensity and percentage positivity of the cells, as determined by the two pathologists, were then averaged and multiplied to generate the immunoreactivity score (IS) for each case as follows: $\sum(0 \times F0 + 1 \times F1 + 2 \times F2 + 3 \times F3)$.

For the histological analysis, the sections of mouse calvaria were heated at 60 °C for 2 h and then put in xylene for 20 min and successively dehydrated with 100% ethanol, 95% ethanol, and 75% ethanol for 5 min followed by washing with PBS 3 times. Hematoxylin and eosin (H&E) staining was performed using a H&E staining kit (C0105, Beyotime Biotechnology),

according to the manufacturer's instructions. Tartrate-resistant acid phosphatase (TRAP) staining was performed using a TRAP staining kit (D023-1-1, Nanjing Jiancheng Bioengineering Institute), according to the manufacturer's instructions. Neutral balsam was used for mount preparation, and a biomicroscope (DM2000, Leica) was used for observation. The erosion area was determined by tracing the area of soft tissue between the parietal bones, including resorption pits on the superior surface of the calvaria. The presence of dark-purple-stained granules in the TRAP-stained section—located on the bone perimeter within a resorption lacuna—indicated osteoclasts.

2.2 TiPs and lipopolysaccharide (LPS)

TiPs (<20 μm, W08A030, Alfa Aesar) were diluted with pure water and then filtered by Isopore membrane filters (pore size: 10/1.2/0.2 μm, TCTP04700/RTTP04700/GTTP04700, Millipore) in filter holders, and TiPs (average diameter: 15.47 ± 5.18, 3.75 ± 1.08, and 0.82 ± 0.12 μm), respectively, which were labeled as Ti10, Ti1.2, and Ti0.2, respectively, in this study. TiPs were dried and steeped in 75% ethanol for 48 h and then washed 4 times with sterile ultrapure water, followed by firing at 180 °C for 6 h. TiPs were suspended in PBS, adjusting to a concentration of 9×10^{-3} g mL^{-1}, for *in vitro* experiments. The endotoxin level of TiPs was determined (<0.25 EU ml^{-1} with a Limulus assay—EC80545, Bioendo).

LPS was obtained from Sigma-Aldrich (L2880), and it was dissolved in PBS, adjusting to a concentration of 1 μg ml^{-1}, for *in vitro* experiments.

2.3 Cell culture

Bone-marrow-derived macrophages (BMDMs) were obtained by differentiating bone marrow progenitors from the tibia and femur of 8-week-old C57BL/6J male mice in high-glucose Dulbecco's modified Eagle's medium (DMEM) (C11995500BT, Thermo Fisher Scientific) containing 10% fetal bovine serum (FBS) (10099141, Thermo Fisher Scientific), 10 ng ml^{-1} recombinant M-CSF (51112-MNAH, Sino Biological Inc), penicillin, and streptomycin (SV30010, Thermo Fisher Scientific) for 7 d. RAW264.7 macrophages and HEK293T cells were obtained from Procell Life Science & Technology Co., Ltd, and they were grown in high-glucose DMEM containing 10% FBS. All the cells were cultured at 37 °C and 5% CO_2. Both BMDMs and RAW264.7 macrophages were seeded 1 d before the experiments using high-glucose DMEM containing 10% FBS, penicillin, and streptomycin. Cell counters (Countstar BioTech) were used with 98% viability in all the trials.

2.4 Total RNA extraction and real-time PCR

Total RNA was extracted from the cells using RNAiso Plus (9109, TaKaRa Biotechnology), and the RNA concentration was measured by a NanoDrop instrument (ND-2000, Thermo Fisher Scientific). PrimeScript RT Master Mix (RR036D, TaKaRa Biotechnology) was used to reverse-transcribe RNA to cDNA. Real-time PCR was performed using UNICONTM qPCR SYBR Green Master Mix (11198ES08, Yeasen) and a LightCycler 96 real-time PCR system (Roche Molecular Systems, Inc.). GAPDH was used as the housekeeping gene. All the reactions were run in triplicate. The primers of the target genes are listed in Table 1.

Table 1 Primers used in this study

ZBTB20	Forward	GTGGACCGAATCTACTCCGC
	Reverse	CATGAATGCGTGTGATCCAGC
iNOS	Forward	GGAGTGACGGCAAACATGACT
	Reverse	TCGATGCACAACTGGGTGAAC
COX-2	Forward	TGCACTATGGTTACAAAAGCTGG
	Reverse	TCAGGAAGCTCCTTATTTCCCTT
IL-6	Forward	CTGCAAGAGACTTCCATCCAG
	Reverse	AGTGGTATAGACAGGTCTGTTGG
TNF-α	Forward	CCTGTAGCCCACGTCGTAG
	Reverse	GGGAGTAGACAAGGTACAACCC
GAPDH	Forward	TGTGTCCGTCGTGGATCTGA
	Reverse	TTGCTGTTGAAGTCGCAGGAG

2.5 TNF-α, IL-6, and interferon-β (IFN-β) measurements by using instant ELISA

At the described time points after stimulation, cell supernatants were harvested and centrifuged to remove the cellular debris. Then, the excreted TNF-α, IL-6, and IFN-β were detected using an instant enzyme-linked immunosorbent assay (ELISA) kit (EMC102a.96/EMC004.96/EMC016.96, Neobioscience Technology Co., Ltd), according to the manufacturer's instructions.

2.6 Western blot

BMDMs were seeded in 6-well plates at a density of 2×10^5 cells per well. After 24 h, BMDMs were stimulated with TiPs or LPS and then BMDMs were lysed by a RIPA buffer (9806S, Cell Signaling Technology) with PMSF (P0100-1, Solarbio) and phosphatase inhibitor cocktail (CW2383, CW Biotech).

Lysates were centrifuged at 12 000*g* for 15 min, and the supernatants were collected. A bicinchoninic acid (BCA) protein assay (23225, Thermo Fisher Scientific) was used to determine the protein concentrations. The protein samples were separated by SDS-PAGE using 10% polyacrylamide gel and transferred to polyvinylidene fluoride (PVDF) membranes (3010040001, Sigma-Aldrich). Five percent BSA in TBS-Tween (CW0043S, CW Biotech) was used to block the PVDF membranes at 20 °C for 1 h. The membranes were cut into small pieces according to different protein molecular masses and then probed with the relevant antibodies overnight at 4 °C. The antibodies used were p-IKKβ (rabbit, 2697, Cell Signaling Technology), IKKβ (rabbit, 8943, Cell Signaling Technology), p-p65 (rabbit, 3033, Cell Signaling Technology), p65 (rabbit, 8242, Cell Signaling Technology), p-IκBα (rabbit, 2859, Cell Signaling Technology), IκBα (mouse, 4814, Cell Signaling Technology), GAPDH (rabbit, 5174, Cell Signaling Technology), p-IRF3 (rabbit, 29047, Cell Signaling Technology), IRF3 (rabbit, ab68481, Abcam), ZBTB20 (rabbit, NBP2-20936, Novus Biologicals), p-JNK (rabbit, 4668, Cell Signaling Technology), p-ERK (rabbit, 4370, Cell Signaling Technology), p-p38 (rabbit, 4511, Cell Signaling Technology), and histone H3 (rabbit,

4499, Cell Signaling Technology). The membranes were detected with HRP-linked secondary antibodies (goat anti-rabbit, 7074; horse anti-mouse, 7076; Cell Signaling Technology), super ECL detection reagent (36208ES60, Yeasen), and a digital imaging system (Gel Logic 2200 Pro, Kodak).

2.7 Immunofluorescence (IF) staining

BMDMs were seeded at a density of 1×10^5 cells per confocal dish (BDD011035, Jet Bio-Filtration Co., Ltd); 24 h later, TiPs were added. At the described time points after stimulation, BMDMs were immersed in 4% PFA at 20 °C for 15 min. Then, the BMDMs were treated with 0.1% Triton X-100 in PBS and gently shaken at 20 °C for 15 min. Thereafter, BMDMs were blocked in 1% BSA and gently shaken at 20 °C for 30 min, followed by incubation with TNF-α antibody (rabbit, 11948, Cell Signaling Technology), IL-6 antibody (rabbit, 21865-1-AP, Proteintech), p65 antibody (rabbit, 8242, Cell Signaling Technology), IRF3 antibody (rabbit, ab68481, Abcam), TGN38 antibody (mouse, MA3-063, Thermo Fisher Scientific), and p230 antibody (rabbit, sc-102565, Santa Cruz Biotechnology) overnight at 4 °C. Then, the BMDMs were washed with PBS 3 times, followed by incubation with secondary IF antibodies (goat anti-rabbit, A32740; goat anti-mouse, A32723, Thermo Fisher Scientific) at 20 °C for 1 h. After washing three times with PBS, the BMDMs were treated with antifade fluorescence mounting medium with DAPI (HNFD-02, HelixGen Co., Ltd) and covered with microscope cover glasses (T_7011254580, Thermo Fisher Scientific). Finally, the BMDMs were imaged by confocal microscopy (LSM 710, Carl Zeiss).

The sections of C57BL/6J male mouse calvaria were heated at 37 °C for 1 h and at 60 °C for 1 h and then put in xylene for 20 min and sequentially dehydrated with 100% ethanol, 95% ethanol, and 75% ethanol for 5 min, followed by washing with PBS 3 times. Antigen retrieval was performed with pepsin at 37 °C for 30 min, followed by washing with PBS 3 times. Five percent BSA was used as a blocking buffer at 20 °C for 2 h; then, the sections were incubated with the relevant antibodies overnight at 4 °C. The antibodies included TNF-α (rabbit, A11543, Abclonal), CD206 (rabbit, 18704-1-AP, Proteintech), and iNOS (rabbit, 13120, Cell Signaling Technology). Then, the sections were washed 3 times with PBS followed by incubation with secondary IF antibodies (goat anti-rabbit, A32740/35552, Thermo Fisher Scientific) at 20 °C for 1 h. After washing three times with PBS, the BMDMs were treated with antifade fluorescence mounting medium with DAPI and covered with microscope cover glasses. Finally, the sections were imaged by fluorescence microscopy (BX63, Olympus).

2.8 Flow cytometry

The BMDMs were seeded in 6-well plates at a concentration of 5×10^5 cells per well. Twenty-four hours after seeding, the BMDMs were stimulated by TiPs for 24 h and then treated with TrypLE Express Enzyme (12604021, Thermo Fisher Scientific) to remove them from the plates. Then, the BMDMs were centrifuged at 1000 rpm for 5 min. Following our recent study protocol,[12] after washing in PBS, the BMDMs were incubated with APC-conjugated CD206 antibody (17-2061-82, Thermo Fisher Scientific) at 20 °C for 20 min in the dark. Then, the BMDMs were washed with PBS and incubated with a fixation buffer (00-8222-49, Thermo Fisher Scientific) at 20 °C for 20 min in the dark. After washing with Perm/Wash buffer (554723, BD Biosciences), the BMDMs were incubated with PE-cyanine7-conjugated iNOS antibody (25-5920-82, Thermo Fisher Scientific) at 20 °C for 20 min in the dark. The isotype controls used were APC-conjugated rat IgG2b,κ (17-4031-82, Thermo Fisher Scientific) and PE-cyanine7-conjugated rat IgG2a,κ (25-4321-82, Thermo Fisher Scientific). After washing with the Perm/Wash buffer, the BMDMs were suspended in PBS and analyzed using flow cytometry (BD FACSVerse, BD Biosciences).

2.9 Plasmids, siRNAs, viruses, and stable cell lines

The plasmid-expressing mouse *Zbtb20* (Gene ID: 56490) (ZBTB20-expressing plasmid), as well as the siRNA-sequences-targeting mouse *Zbtb20* (ZBTB-siRNA) and mouse *IκBα* (Gene ID: 18305) (IκBα-siRNA), were designed and synthesized by GenePharma. The mock vehicle and negative control siRNA (NC-siRNA) were considered to be the controls. The siRNA sequences are listed in Table 2.

The recombinant lentiviruses for mouse *Zbtb20* expressing (ZBTB20-expressing lentivirus) and mouse *Zbtb20* interfering (sh-ZBTB20 lentivirus) with mock lentivirus and NC lentivirus, respectively, as the controls were synthesized by GenePharma. The lentivirus expressing firefly luciferase (fluc-lentivirus) was obtained from OBiO Technology.

To fabricate a promoter luciferase reporter plasmid, the genomic DNA was isolated from RAW264.7 macrophages using a genomic DNA isolation kit (ab65358, Abcam). The 2.1 kb mouse *IκBα* promoter (−2000/+121 *IκBα*-Luc) was amplified by PCR and then subcloned into the pGL3-basic luciferase vector

Table 2 Sequences of ZBTB20-siRNAs and IκBα-siRNAs

Sequence	Gene sequence (5′ to 3′)
ZBTB20-537	CUAGAACGGAAGAAACCCATT
	UGGGUUUCUUCCGUUCUAGTT
ZBTB20-721	GGUCAUCUGAUUGUGACAUTT
	AUGUCACAAUCAGAUGACCTT
ZBTB20-1391	CUGGAUCACACGCAUUCAUTT
	AUGAAUGCGUGUGAUCCAGTT
ZBTB20-1953	CAGCUCUAUUUACGCCAGATT
	UCUGGCGUAAAUAGAGCUGTT
IκBα-233	GGACGAGGAGUACGAGCAAAU
	UUGCUCGUACUCCUCGUCCUU
IκBα-2296	GAGGGAUUUCAGUUGUUUAAC
	UAAACAACUGAAAUCCCUCUG
IκBα-2885	GGCUGUUGUCUUUGUGAAAUC
	UUUCACAAAGACAACAGCCGA
IκBα-3193	GGUACUUCUAAGAUGUAUAUU
	UAUACAUCUUAGAAGUACCAA
Negative control	UUCUCCGAACGUGUCACGUTT
	ACGUGACACGUUCGGAGAATT
GAPDH	CACUCAAGAUUGUCAGCAATT
	UUGCUGACAAUCUUGAGUGAG

(Promega) to yield a promoter luciferase reporter plasmid (IκBα-promoter-luciferase plasmid). Further, the pRL-TK-Renilla-luciferase plasmid was obtained from Promega. All the constructs were confirmed by DNA sequencing.

The BMDMs were seeded in 6-well plates at a concentration of 5×10^5 cells per well; 24 h later, the BMDMs were cultured in Opti-MEM I reduced-serum medium (31985070, Thermo Fisher Scientific) for 12 h. Thereafter, the BMDMs were transfected with 200 pmol siRNA using 7.5 μl Lipofectamine RNAiMAX transfection reagent (13778075, Thermo Fisher Scientific) in each well. The medium was replaced with high-glucose DMEM containing 10% FBS 8 h after transfection. Then, the BMDMs were cultured for another 48 h before subsequent experiments.

RAW264.7 macrophages were seeded in 6-well plates at a concentration of 5×10^5 cells per well. Twenty-four hours later, RAW264.7 macrophages were incubated in 1×10^7 transducing unit (TU) per mL lentivirus for 12 h, including ZBTB20-expressing lentivirus, mock lentivirus, sh-ZBTB20 lentivirus, NC lentivirus, and fluc-lentivirus. Subsequently, these RAW264.7 macrophages were cultured in high-glucose DMEM containing 10% FBS for 72 h before further experiments, and ZBTB20-expressing-RAW264.7, mock-RAW264.7, sh-ZBTB20-RAW264.7, and NC-RAW264.7 were respectively obtained. The RAW264.7 macrophages transfected with fluc-lentivirus were used as the bioluminescent reporter cells.

2.10 RNA-seq

The RAW264.7 macrophages were stimulated by TiPs for 4 h and the total RNA was isolated using RNAiso Plus. For strand-specific library construction and sequencing, the rRNAs were removed to retain mRNAs and ncRNAs, which were then fragmented and reverse-transcribed into cDNA with random primers. Second-strand cDNA were synthesized using dUTP and purified with a QIAquick PCR purification kit (28104, Qiagen). Then, the second-strand cDNA were end-repaired, poly (A) was added, and then they were ligated to Illumina sequencing adapters. Uracil-*N*-glycosylase (UNG) was subsequently used to digest the second-strand cDNA. The digested products were size-selected by agarose gel electrophoresis and amplified by PCR. The sequencing was carried out on an Illumina HiSeq 4000 instrument. For bioinformatics analysis, raw reads containing the adapter or having low quality (*Q*-value ≤20) were removed and then mapped to the mouse reference genome (GRCm38) by using HISAT2 (version 2.1.0). The resulting files were sorted using SAMtools and analyzed *via* HTSeq (version 0.9.0) to determine the counts of each gene. For differential expression analysis, the gene abundances were quantified by the R package edgeR. Here, FDR < 0.05 and log 2 (fold change) >1 were used as the thresholds to define significant differentially expressed genes (DEGs). Gene set enrichment analysis (GSEA) was performed using the software obtained from http://software.broadinstitute.org/gsea. Gene ontology (GO) and Kyoto Encyclopedia of Genes and Genomes (KEGG) pathway analyses of DEGs were performed using the R package clusterProfiler.

2.11 Dual-luciferase reporter assay

HEK293T cells were cotransfected with IκBα-promoter-luciferase plasmid, pRL-TK-Renilla-luciferase plasmid, and ZBTB20-expressing plasmid. The total amounts of the plasmids were equalized with the mock vehicle. After 48 h, the Dual-Luciferase Reporter Assay System (E1910, Promega) was used to measure the Firefly and Renilla luciferase activities according to the manufacturer's instructions. To normalize with respect to transfection efficiency, firefly luciferase activity was divided with the Renilla luciferase activity. All the analyses were performed in triplicate.

2.12 Animal surgery

Male C57BL/6J mice aged 8 weeks and male nude mice aged 8 weeks were purchased from the Animal Laboratory of Sun Yat-sen University and then raised in specific pathogen-free conditions in Sun Yat-sen University. All the mice were aged 10 weeks at the time of surgery. All the animal procedures were performed in accordance with the guidelines for the care and use of laboratory animals of Sun Yat-sen University and approved by the Animal Ethical and Welfare Committee of Sun Yat-sen University.

For the *in vivo* experiments on C57BL/6J mice, the mice were randomly divided into six groups: (i) control (Control) group, (ii) TiPs (Ti) group, (iii) NC lentivirus + TiPs (NC + Ti) group, (iv) sh-ZBTB20 lentivirus + TiPs (sh-ZBTB20 + Ti) group, (v) mock lentivirus + TiPs (Mock + Ti) group, and (vi) ZBTB20-expressing lentivirus + TiPs ($ZBTB20^+$ + Ti) group; there were eight C57BL/6J mice in each group. The male C57BL/6J mice were anesthetized by using 10% chloral hydrate (0.1 milliliter per kilogram of body weight) *via* intraperitoneal injection. Then, 15 mm midline sagittal incisions on the heads of the C57BL/6 mice were made to expose the calvaria. A 0.5 × 0.5 × 0.5 cm^3 gelatin sponge was placed over the calvaria. In the Control group, 100 μl PBS was locally injected at the sagittal midline of the calvaria before suturing. In the Ti group, 100 μl PBS containing 3 mg Ti0.2 was locally injected at the sagittal midline of the calvaria before suturing. In the NC + Ti, sh-ZBTB20 + Ti, Mock + Ti, and $ZBTB20^+$ + Ti groups, 30 μl PBS containing 3 mg Ti0.2 and corresponding 70 μl shRNA lentivirus (titer: 1×10^8 TU mL^{-1}) were locally injected at the sagittal midline of the calvaria before suturing. No death or complications were observed during the 7 days of observation after the operation. Then, the C57BL/6 mice were euthanized, and their calvaria were harvested with all the soft tissues removed for micro-CT imaging, IHC assay, and histological analysis.

For the *in vivo* experiments on nude mice, the male nude mice were randomly divided into seven groups: (i) bioluminescence (BLI) group, (ii) control (Control) group, (iii) TiPs (Ti) group, (iv) NC-RAW264.7 + TiPs (NC + Ti) group, (v) sh-ZBTB20-RAW264.7 + TiPs (sh-ZBTB20 + Ti) group, (vi) mock-RAW264.7 + TiPs (Mock + Ti) group, and (vii) ZBTB20-expressing-RAW264.7 + TiPs ($ZBTB20^+$ + Ti) group; there were eight nude mice in each group. The male nude mice were anesthetized by using 10% chloral hydrate (0.1 milliliter per

kilogram of body weight) *via* intraperitoneal injection. Then, 15 mm midline sagittal incisions on the heads of the nude mice were made to expose the calvaria. A 0.5 × 0.5 × 0.5 cm^3 gelatin sponge was placed over the calvaria. In the BLI group, 100 μl PBS containing 0.5 × 10^6 bioluminescent reporter cells were locally injected at the sagittal midline of the calvaria before suturing. In the Control group, 100 μl PBS was locally injected at the sagittal midline of the calvaria before suturing. In the Ti group, 100 μl PBS containing 3 mg Ti0.2 was locally injected at the sagittal midline of the calvaria before suturing. In the NC + Ti, sh-ZBTB20 + Ti, Mock + Ti, and ZBTB20$^+$ + Ti groups, 100 μl PBS containing 3 mg Ti0.2 and corresponding 0.5 × 10^6 stably transfected RAW264.7 macrophages were locally injected at the sagittal midline of the calvaria before suturing. No death or complications were observed during the 7 days of observation after the operation. Then, the nude mice were euthanized, and their calvaria were harvested with all the soft tissues removed for micro-CT imaging.

2.13 Bioluminescence imaging

As mentioned above, bioluminescent reporter cells were locally injected at the sagittal midline of the calvaria of nude mice. Luciferase substrate D-luciferin (40901ES03, Yeasen) was intraperitoneally injected (3 mg per nude mouse); 10 min later, the bioluminescence images were taken. The nude mice were immediately imaged after the operation (day 0) and then imaged every day for a week (day 7) using a bioluminescence imaging system (IVIS Lumina LT Series III, PerkinElmer). After imaging at day 7, these nude mice were euthanized.

2.14 Micro-CT

After the calvaria were harvested, micro-CT scans were performed using a high-resolution *in vivo* micro-CT imaging system (ZKKS-MCT-Sharp, Zhongke Kaisheng Medical Technology) and associated software (ZZKS-Micro-CT4.1). The radiographic projections were acquired at 60 kV and 667 μA within 240 ms. All the projection frames were recorded five times and then averaged. The 3D images were reconstructed using the bundled manufacturer's reconstruction software. Bone mineral density (BMD), bone volume (BV), total volume (TV), and BV/TV were measured from a 1 × 3 × 3 mm^3 region of interest in the cross-section slices around the sagittal suture according to our earlier studies.[13]

2.15 Statistics

All the results were from at least three independent experiments. The data are expressed as mean ± standard deviation (SD). All the values were first assessed using the Kolmogorov–Smirnov test to verify data normality. Two-sided Student's *t*-test was utilized between two groups. One-way analysis of variance (ANOVA) was utilized among three or more than three groups, and Fisher's least significant difference (LSD) test was used for *post hoc* comparisons. Statistical analyses were performed with the SPSS 20.0 software, and $p < 0.05$ was considered to be statistically significant.

3. Results

3.1 TNF-α and IL-6 were upregulated in synovial membranes around aseptic loosening prostheses

To investigate the relationship between AL and inflammation, we performed H&E staining and IHC on synovial membranes. As shown in the H&E-stained sections (Fig. 1A), wear particles could be observed in the H&E staining in the AL group rather than the Control group. Meanwhile, the brown color represented the staining intensities of TNF-α and IL-6 expressed in cytoplasm, and the expression levels of TNF-α and IL-6 in the AL group were higher than those in the Control group. With regard to the IS for each group, the average IS values of TNF-α and IL-6 in the AL group were 1.90 ± 0.17 and 2.41 ± 0.26, respectively, which were significantly higher than the corresponding values in the Control group (0.11 ± 0.10 and 0.10 ± 0.09; $p < 0.05$) (Fig. S1A†).

Macrophages are widely recognized as important mediators of TLR-triggered inflammatory responses. Therefore, we stimulated BMDMs with Ti0.2 for various time periods (1, 2, 4, 6, 12, or 24 h for real-time PCR; 1, 2, or 4 h for ELISA; 4 h for IF staining). As shown in Fig. 1B, TNF-α and IL-6 mRNA levels were upregulated following the addition of Ti0.2 in a time-dependent manner. In addition, the degrees of TNF-α and IL-6 mRNA upregulation were also dependent on the particle diameters, and Ti0.2 caused the highest elevation among the three TiP diameters (Fig. S1B†). Moreover, ELISA revealed that TNF-α and IL-6 secretions were significantly increased at 1, 2, and 4 h after Ti0.2 stimulation ($p < 0.05$) (Fig. 1C). To further confirm the upregulation of cellular TNF-α and IL-6, we examined the expressions of TNF-α and IL-6 in BMDMs *in vitro* by means of IF staining. Confocal microscopy revealed that TiPs could induce the protein production of TNF-α and IL-6 (Fig. 1D). Taken together, these data indicated that TNF-α and IL-6 were upregulated in the synovial membranes around AL prostheses, and TiPs induced the upregulation of TNF-α and IL-6 expressions in BMDMs.

3.2 TiPs induce the activation of NF-κB signaling pathway and phosphorylation of IRF3 in BMDMs

In order to verify the activation mechanism of TiPs, we stimulated BMDMs with Ti0.2 or LPS for different time periods (1 h for NF-κB pathway western blot; 30, 60, or 90 min for nuclear protein p65 western blot; 1 h for p65 translocation IF staining; 4 or 8 h for p-IRF3 and IRF3 western blot; 8 h for IRF3 translocation IF staining; 4 or 8 h for IFN-β ELISA). Both Ti0.2 and LPS significantly increased the protein expressions of p-IKKβ, p-p65, and p-IκBα ($p < 0.05$), with no obvious changes in the total protein expressions of IKKβ, p65, and IκBα (Fig. 2A). Further, the nuclear protein of p65 increased after the indicated stimulation durations of Ti0.2, with the largest increase for the duration of 30 min (Fig. 2B) ($p < 0.05$). IF staining showed that the protein of p65 (red) translocated from the cytoplasm into the nucleus (blue) after Ti0.2 stimulation in BMDMs (Fig. 2C). Cytokines of type I interferon (*e.g.*, IFN-β), which are triggered by the transcription factor IRF3, are impor-

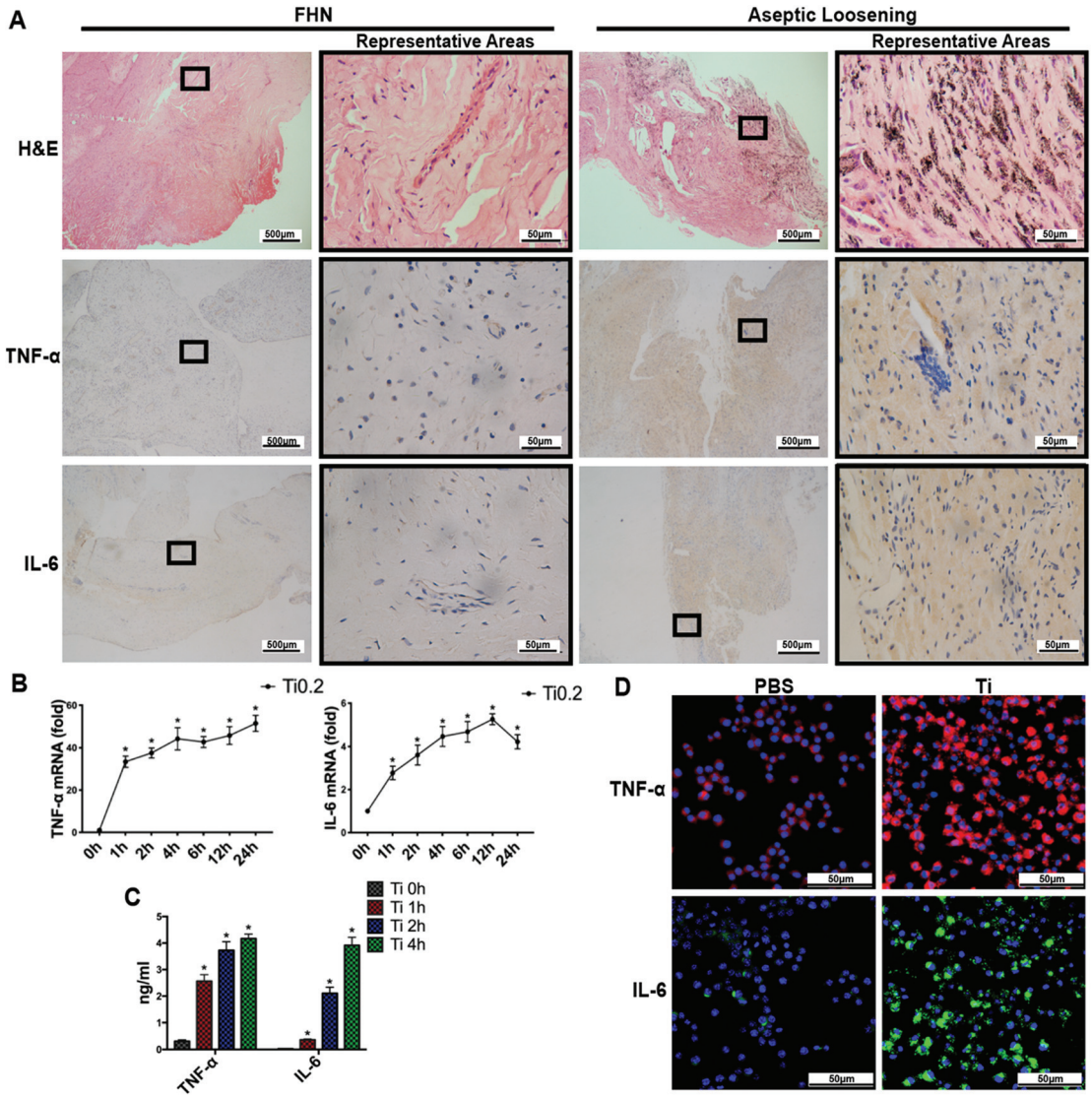

Fig. 1 TNF-α and IL-6 increased in synovial membranes from the AL group and in BMDMs after TiPs stimulation. (A) H&E staining and IHC staining of TNF-α and IL-6 in specimens from AL and FHN patients. (B) mRNA expression of TNF-α and IL-6 in BMDMs were significantly upregulated after stimulation by Ti0.2 at every time point ($p < 0.05$). (C) Cytokines of TNF-α and IL-6 secreted by BMDMs significantly increased after stimulation with Ti0.2 for the indicated time durations (TNF-α: 1 h, 2.56 ± 0.28 ng ml^{-1}; 2 h, 3.73 ± 0.27 ng ml^{-1}; 4 h, 4.17 ± 0.19 ng ml^{-1} *vs.* 0 h, 0.31 ± 0.06 ng ml^{-1}, $p < 0.05$. IL-6: 1 h, 0.37 ± 0.03 ng ml^{-1}; 2 h, 2.11 ± 0.26 ng ml^{-1}; 4 h, 3.91 ± 0.32 ng ml^{-1} *vs.* 0 h, 0.03 ± 0.01 ng ml^{-1}, $p < 0.05$). (D) TiPs induced the production of TNF-α and IL-6 in BMDMs (red: TNF-α; green: IL-6; blue: nucleus). *$p < 0.05$. Statistical significance was determined by one-way ANOVA with Fisher's LSD test. All the data are shown as mean ± SD. The assays were performed at least three times for each sample.

tant to induce the M1 macrophage phenotype. To investigate whether TiPs induced the activation of IRF3, western blot was performed; we observed increased levels of p-IRF3, but not the total IRF3 levels, after TiPs stimulation in BMDMs ($p < 0.05$) (Fig. 2D). To further confirm the IRF3 activation mechanism by TiPs, we examined the location of IRF3 in BMDMs by IF staining. Confocal microscopy revealed that TiPs induced IRF3 (yellow) translocation from the cytoplasm to the nucleus (blue) (Fig. 2E). Moreover, ELISA yielded a similar result: the secreted IFN-β was significantly increased at 4 or 8 h after Ti0.2 stimulation ($p < 0.05$) (Fig. 2F). Quantitative analyses of the western blot results are shown in Fig. S2.† Collectively, these results indicated that TiPs activated the NF-κB signaling pathway and IRF3, leading to the production of proinflammatory factors, such as IFN-β cytokines.

3.3 RNA-seq analysis revealed that ZBTB20 correlates with TiPs-induced inflammation in macrophages *via* IκBα

We generated the mRNA profiles of RAW264.7 macrophages pretreated with Ti0.2 for 4 h by RNA-seq using Illumina HiSeq 4000. We performed a heat map and cluster analysis (Fig. 3A and B). A total of 194 upregulated mRNAs and 72 downregulated mRNAs were profiled (log 2 FC > 1, FDR < 0.05). To verify the relations and connections between these DEGs, GO and

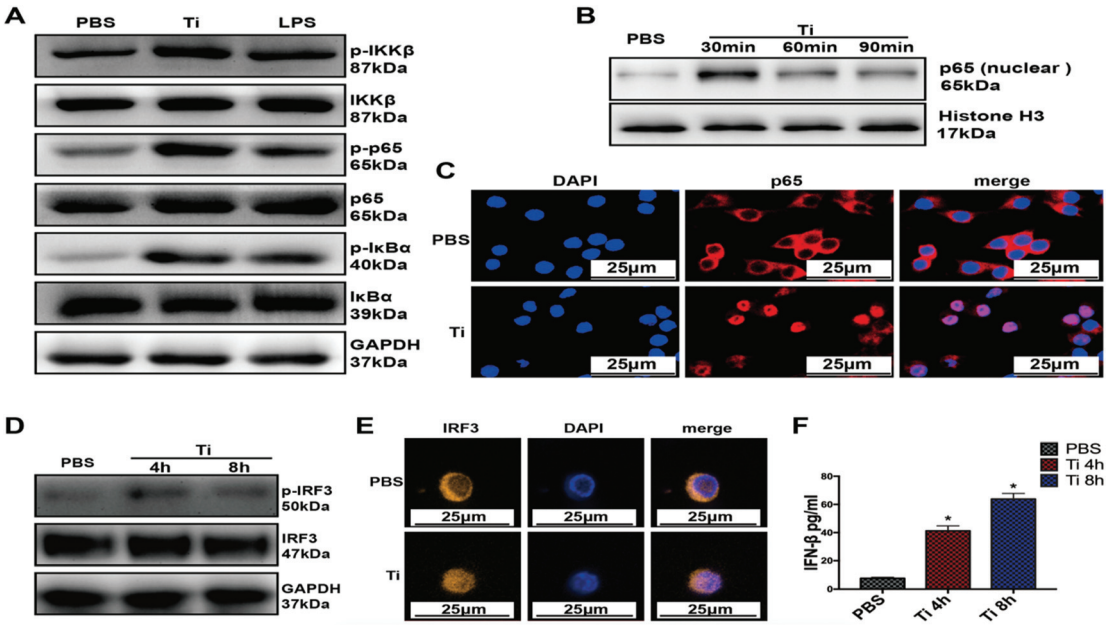

Fig. 2 TiPs induce the activation of NF-κB signaling pathway and phosphorylation of IRF-3 in BMDMs. (A) Protein concentrations of p-IKKβ, p-p65, and p-IκBα increased in the BMDMs after Ti0.2 or LPS (1 μg ml^{-1}) stimulation for 1 h ($p < 0.05$). (B) Nuclear protein p65 of BMDMs increased after Ti0.2 stimulation for 30, 60, or 90 min ($p < 0.05$). (C) p65 protein (red) translocated from the cytoplasm into the nucleus (blue) after Ti0.2 stimulation for 1 h in BMDMs. (D) Ti0.2 induced the phosphorylation of IRF-3 at the indicated time points ($p < 0.05$). (E) After pretreatment with Ti0.2 for 8 h, IRF3 (yellow) aggregated into the nucleus (blue) in BMDMs. (F) Secreted IFN-β was significantly increased after Ti0.2 stimulation for 4 or 8 h ($p < 0.05$). *$p < 0.05$. Statistical significance was determined by one-way ANOVA with Fisher's LSD test. All the data are shown as mean ± SD. The assays were performed at least three times for each sample.

KEGG pathway analyses were performed. The 266 DEGs were annotated using GO categories and the KEGG database: the top 15 significant GO terms and pathways are shown (Fig. S3A†). Moreover, GSEA revealed four important KEGG pathways: cytokine–cytokine receptor interaction, nod-like receptor signaling pathway, toll-like receptor signaling pathway, and hematopoietic cell lineage enriched in TiPs-stimulated RAW264.7 macrophages (Fig. S3B†). Each of the four pathways contained specific core enrichment genes, and the Venn diagram of the four pathways' core enrichment genes showed that TNF-α, IL-6, and IL-1β intersected (Fig. 3C). The protein–protein interaction network (PPIN) from the STRING database showed that IκBα was a potential upstream target of TNF-α, IL-6, and IL-1β, which indicated that IκBα was crucial in TiPs-induced inflammation (Fig. 3D). Importantly, we found that transcription factor ZBTB20 was bound to a specific promoter site according to the Animal Transcription Factor Database (http://bioinfo.life.hust.edu.cn) (Fig. S3C†), and ZBTB20 has an activity of gene transcription suppression, such as *Afp*, *Sox9*, and *IκBα* (Fig. 3E). In brief, our RNA-seq analysis results suggested that ZBTB20 correlates with TiPs-induced inflammation in macrophages *via* IκBα.

3.4 ZBTB20 positively regulates TiPs-induced inflammatory response in BMDMs

To investigate the relationship between ZBTB20 and synovial membrane inflammation, we performed IHC on synovial membranes. The IHC assessment of synovial membranes showed that the cytoplasm protein expression of ZBTB20 increased in the AL group when compared with that in the FHN group (Fig. 4A). The average IS value of ZBTB20 in the AL group was 1.93 ± 0.33, which was significantly higher than that in the FHN group (0.09 ± 0.05, $p < 0.05$) (Fig. S4A†).

To determine the connection between ZBTB20 and TiPs-induced macrophage activation, we stimulated BMDMs with TiPs for different time periods (4, 8, 12, or 24 h for ZBTB20 real-time PCR; 12, 24, or 36 h for ZBTB20 western blot; 6 h for TNF-α and IL-6 ELISA; 4 h for TNF-α and IL-6 real-time PCR; 4 h for TNF-α and IL-6 IF staining). The mRNA and protein expressions of ZBTB20 in BMDMs was upregulated after stimulation by Ti0.2 at every time point ($p < 0.05$) (Fig. 4B and C). To further investigate the effect of ZBTB20 knockdown/overexpression on proinflammatory cytokines production by TiPs-activated BMDMs, we synthesized four siRNA-sequences-targeting mouse *Zbtb20* and plasmid-expressing mouse *Zbtb20*. The endogenous mRNA and protein expressions of ZBTB20 in BMDMs were markedly diminished by ZBTB20-siRNA (Fig. S4B and C†), but obviously increased by ZBTB20-expressing plasmids (Fig. S4D and E†). ZBTB20 knockdown resulted in significantly lower cytokines production of TNF-α and IL-6 induced by Ti0.2 in BMDMs ($p < 0.05$) (Fig. 4D). Correspondingly, ZBTB20 overexpression promoted the cytokines production of TNF-α and IL-6 induced by Ti0.2 in BMDMs ($p < 0.05$) (Fig. 4E). Similar trends were observed in the mRNA expression

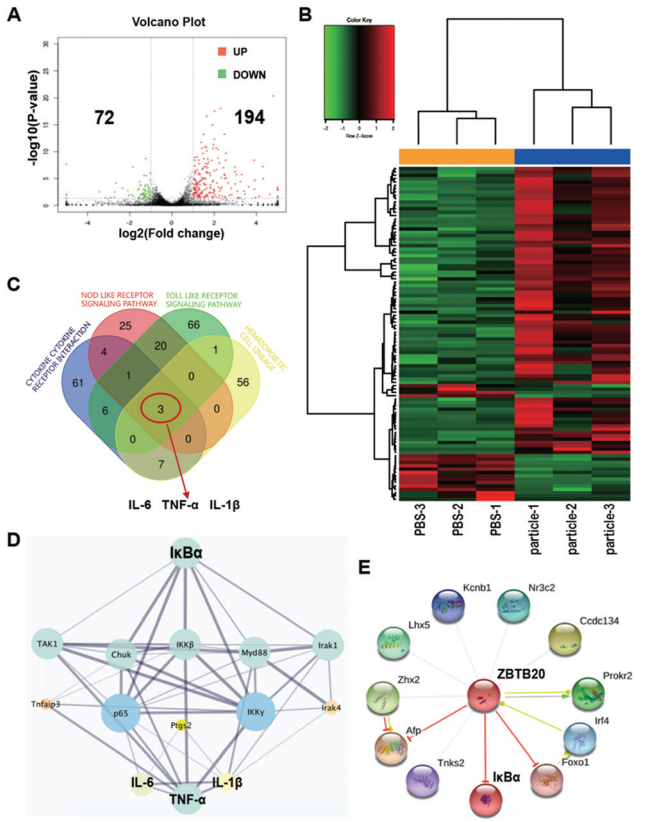

Fig. 3 RNA-seq analysis revealed that ZBTB20 correlates with TiPs-induced inflammation in macrophages *via* IκBα. (A) Volcano plot reveals 194 upregulated genes and 72 downregulated genes in RAW264.7 after Ti0.2 stimulation for 4 h. (B) Heat map and cluster analysis. (C) Venn diagram of the four crucial KEGG pathways obtained from the GSEA analysis revealed that TNF-α, IL-6, and IL-1β played important roles in TiPs-induced inflammation in RAW264.7. (D) PPIN showed that IκBα was a key upstream target for TNF-α, IL-6, and IL-1β. (E) ZBTB20 exhibits the activity of gene transcription suppression toward *Afp*, *Sox9*, and *IκBα*.

of TNF-α and IL-6 in BMDMs (Fig. S4F and G†). Next, to further confirm the effect of ZBTB20 knockdown on cellular TNF-α, we examined the protein expression of TNF-α in BMDMs by IF staining. Confocal microscopy revealed that ZBTB20-siRNA resulted in remarkably lower cellular TNF-α (red) and IL-6 (green) concentrations in BMDMs stimulated with Ti0.2 (Fig. 4F). Therefore, these data suggest that ZBTB20 positively regulates TiPs-induced inflammatory responses in BMDMs.

3.5 ZBTB20 positively regulates TiPs-induced NF-κB activation in BMDMs by repressing IκBα gene transcription

To further investigate the effect of ZBTB20 knockdown on TiPs-induced macrophage activation, we stimulated BMDMs for different time periods (Ti0.2 or LPS for 1 h for NF-κB pathway western blot; Ti0.2 for 1 h for IF staining of p65; Ti0.2 for 1 h for nuclear protein p65 western blot; Ti0.2 for 0.5, 1, 2, 4, or 6 h for the real-time PCR of IκBα; Ti0.2 for 6 h for the ELISA of TNF-α and IL-6; Ti0.2 for 4 h for the IF staining of TNF-α and IL-6; Ti0.2 for 30 or 60 min for MAPK pathway western blot). western blot analyses revealed that the TiPs-induced phosphorylation of IKKβ (p-IKKβ) and p65 (p-p65) decreased in ZBTB20-knockdown BMDMs, while the protein level of IκBα increased in ZBTB20-knockdown BMDMs when compared with those in the NC-siRNA group ($p < 0.05$); no substantial differences were found in the IKKβ, p65, and phosphorylated IκBα (p-IκBα) levels induced by TiPs between the ZBTB20-siRNA and NC-siRNA groups (Fig. 5A); a quantitative analysis of the western blot results is shown in Fig. S5A.† It is generally accepted that a high level of IκBα leads to the reduced translocation of p65 into the nucleus; therefore, we performed IF staining of p65. As shown in Fig. 5B, the TiPs-induced nuclear translocation of p65 was suppressed in the ZBTB20-siRNA group when compared with that in the NC-siRNA group. Similarly, the nuclear protein of p65 induced by TiPs was reduced in the ZBTB20-siRNA group of BMDMs (Fig. S5B and C†). There were no statistical differences among the phosphorylation of JNK (p-JNK), ERK (p-ERK), and p38 (p-p38) induced by TiPs between the two groups (Fig. S5D†).

To further test the relationship of IκBα with ZBTB20, we performed real-time PCR: the obtained data showed that the mRNA expression of IκBα in the ZBTB20-siRNA group was significantly higher than that in the NC-siRNA group at each time point ($p < 0.05$) (Fig. 5C). Considering that ZBTB20 was a transcriptional repressor and it could repress IκBα gene transcription, dual-luciferase reporter assay was used to identify whether ZBTB20 could bind to the IκBα promoter. We cotransfected HEK293T cells with the IκBα-promoter-luciferase plasmid, pRL-TK-Renilla-luciferase plasmid, and ZBTB20-expressing plasmid; 48 h later, we observed that the ZBTB20-expressing plasmid repressed the relative luciferase activity of IκBα-promoter-luciferase plasmid in a dose-dependent manner ($p < 0.05$) (Fig. 5D). To assess whether the antiinflammatory effects caused by ZBTB20 knockdown could be rescued by IκBα knockdown, we constructed stably transfected BMDMs using sh-ZBTB20 lentivirus or NC lentivirus and then transiently transfected these BMDMs with IκBα-siRNA or NC-siRNA; 48 h later, we stimulated the BMDMs with TiPs. ELISA showed that the transient transfection of IκBα-siRNA could rescue the impaired production of TNF and IL-6 caused by ZBTB20 knockdown ($p < 0.05$) (Fig. 5E). Similar trends were observed in the IF staining of TNF-α and IL-6 (Fig. 5F). In short, these data indicated that ZBTB20 positively regulates TiPs-induced NF-κB activation by repressing IκBα transcription.

3.6 ZBTB20 positively regulates TiPs-induced M1 polarization and stabilizes the localization of p230 on the TGN in BMDMs

The modulation of macrophage polarization may also be pivotal to the inflammatory response induced by wear particles, and the activation of NF-κB pathway is responsible for the M1 polarization of macrophages. Since ZBTB20 positively regulates TiPs-induced NF-κB activation, it is interesting to hypothesize that TiPs-induced BMDM polarization could be regulated by ZBTB20. Therefore, we stimulated BMDMs with Ti0.2 for 24 h and confirmed macrophage polarization by flow cytometry using the M1 marker, iNOS, and the M2 marker,

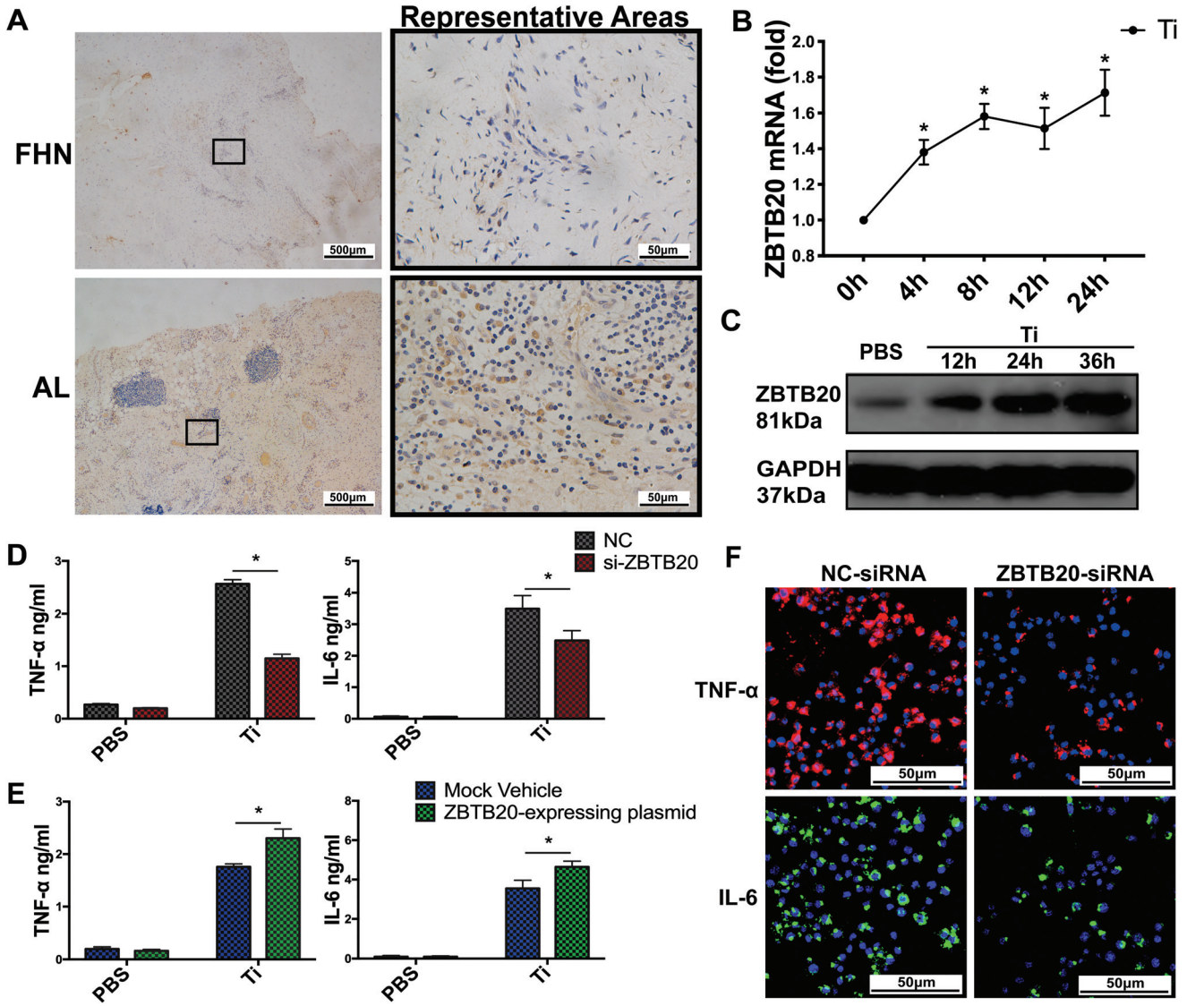

Fig. 4 ZBTB20 positively regulates the TiPs-induced inflammatory response in BMDMs. (A) IHC staining of ZBTB20 in specimens from AL and FHN patients. (B and C) mRNA and protein expressions of ZBTB20 increased in BMDMs after Ti0.2 stimulation at every time point ($p < 0.05$). (D) ZBTB20 knockdown reduced the cytokines production of TNF-α and IL-6 induced by Ti0.2 in BMDMs. (E) ZBTB20 overexpression increased the cytokines production of TNF-α and IL-6 induced by Ti0.2 in BMDMs. (F) ZBTB20 knockdown resulted in remarkably lower cellular TNF-α (red) and IL-6 (green) in BMDMs stimulated with Ti0.2. *$p < 0.05$. Two-sided Student's *t*-test was utilized in (D) and (E). One-way ANOVA with Fisher's LSD test was utilized in (B). All the data are shown as mean ± SD. The assays were performed at least three times for each sample.

CD206. The isotype control is shown in Fig. S6A.† The BMDMs stimulated by PBS functioned as the negative controls, with low percentages of iNOS-positive BMDMs and CD206-positive BMDMs (1.30 ± 0.23% iNOS-positive and 2.89 ± 0.25% CD206-positive in the NC-siRNA + PBS group; 0.99 ± 0.24% iNOS-positive and 2.39 ± 0.42% CD206-positive in the ZBTB20-siRNA + PBS group); there were no significant differences in the iNOS-positive percentages and CD206-positive percentages between the NC-siRNA + PBS and ZBTB20-siRNA + PBS groups. After exposure to TiPs, 26.67 ± 1.57% BMDMs were iNOS-positive in the NC-siRNA + Ti group, while 21.35 ± 1.15% BMDMs were iNOS-positive in the ZBTB20-siRNA + Ti group; meanwhile, 8.38 ± 0.93% BMDMs were CD206-positive in the NC-siRNA + Ti group, while 11.95 ± 0.99% BMDMs were CD206-positive in the ZBTB20-siRNA + Ti group. These flow cytometry data indicate that ZBTB20 knockdown resulted in a decrease in the M1 polarization induced by TiPs by 5.31 ± 0.94% ($p < 0.05$), as well as an increase in the M2 polarization induced by TiPs by 3.57 ± 0.63% ($p < 0.05$) (Fig. 6A and S6B†). Then, we stimulated BMDMs with Ti0.2 for 24 h and used iNOS as the M1 marker and COX-2 as the M2 marker in real-time PCR: similar trends were observed ($p < 0.05$) (Fig. S6B†).

IRF3 is regarded as another critical transcription factor in M1 polarization. To further determine the relationship between ZBTB20 and IRF3, we administered Ti0.2 to BMDMs for 4 or 8 h; further, western blot analyses revealed that the

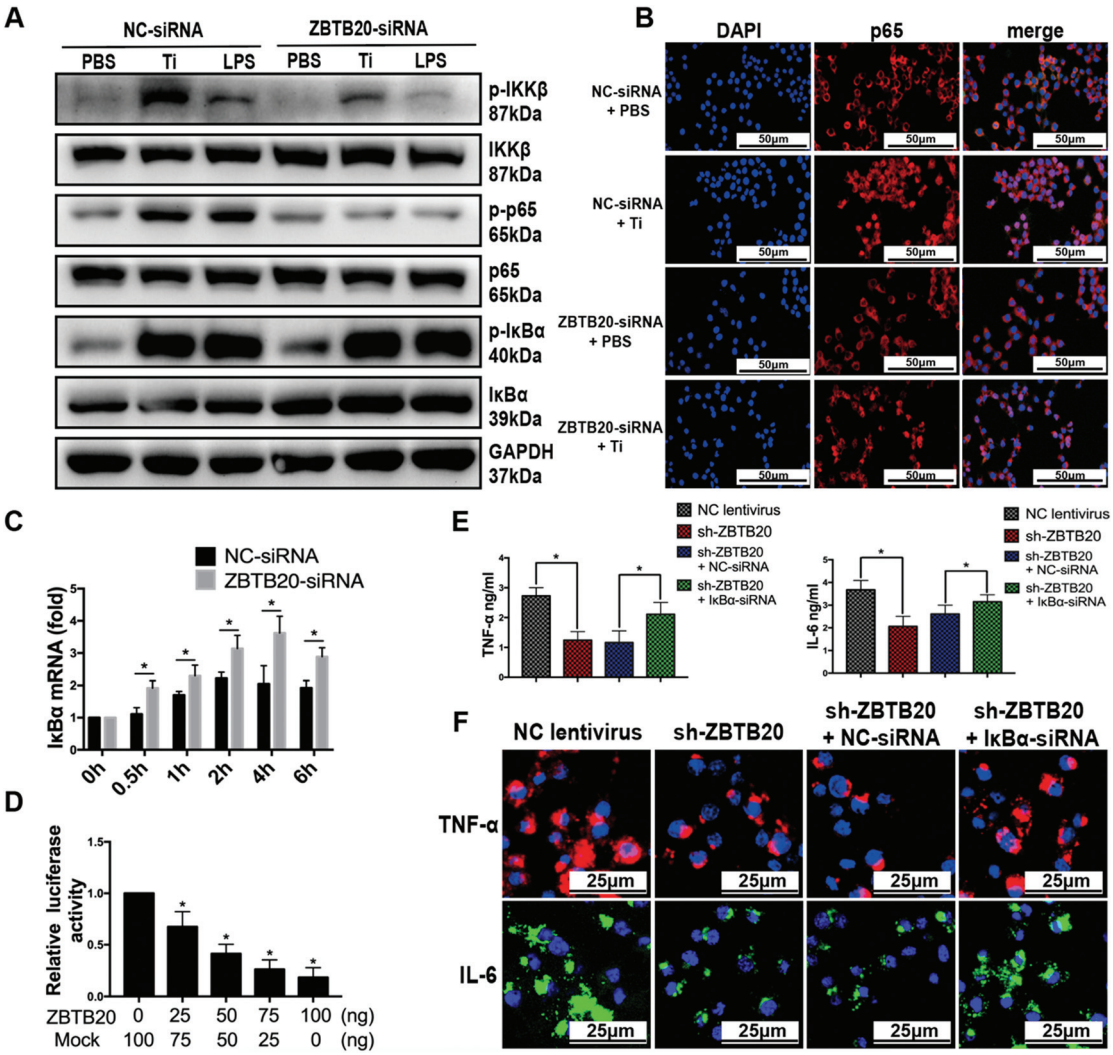

Fig. 5 ZBTB20 positively regulates TiPs-induced NF-κB activation by repressing IκBα transcription. (A) TiPs- or LPS-induced p-IKKβ and p-p65 decreased in ZBTB20-knockdown BMDMs, and the level of IκBα increased in ZBTB20-knockdown BMDMs ($p < 0.05$). (B) TiPs-induced nuclear translocation of p65 was suppressed in the ZBTB20-siRNA group when compared with the NC-siRNA group. (C) mRNA level of IκBα in the ZBTB20-siRNA group was significantly higher than that in the NC-siRNA group at each time point. (D) ZBTB20-expressing plasmid repressed the relative luciferase activity of IκBα-promoter-luciferase plasmid in a dose-dependent manner. (E) IκBα-siRNA rescued the impaired cytokines production of TNF and IL-6 caused by ZBTB20 knockdown. (F) IκBα-siRNA rescued the impaired TiPs-induced cellular TNF (red) and IL-6 (green) caused by ZBTB20 knockdown. *$p < 0.05$. Two-sided Student's *t*-test was utilized in (C). One-way ANOVA with Fisher's LSD test was utilized in (D) and (E). Statistical significance was determined by a two-sided Student's *t*-test. All the data are shown as mean ± SD. The assays were performed at least three times for each sample.

level of IRF3 phosphorylation (p-IRF3) induced by TiPs decreased in the ZBTB20-siRNA group when compared with that in the NC-siRNA group ($p < 0.05$) (Fig. 6B). A quantitative analysis of the western blot results is shown in Fig. S6C.† Next, we stimulated BMDMs with Ti0.2 for 8 h and examined the location of IRF3 by IF staining. Confocal microscopy revealed that the TiPs-induced nuclear translocation of IRF3 was suppressed in the ZBTB20-siRNA group as compared to that in the NC-siRNA group (Fig. 6C). Type I interferon (*e.g.*, IFN-β), which is triggered by IRF3, is important to promote M1 polarization. Therefore, we administered Ti0.2 to BMDMs for 4 or 8 h; ELISA revealed that ZBTB20-siRNA resulted in lower cytokines production of IFN-β induced by TiPs ($p < 0.05$) (Fig. 6D).

Some researchers have found that p230 is a crucial marker of TGN-derived tubular carriers, which transfer cytokines like TNF-α and IFN-β. Our results suggested that ZBTB20 knockdown resulted in lower cytokines production (TNF-α, IL-6, and IFN-β) induced by TiPs in BMDMs; therefore, we attempted to determine the relationship between ZBTB20 and p230. BMDMs were administered with Ti0.2 for 4 h. Confocal microscopy revealed that the binding of p230 (red) to TGN (green) was diminished in the ZBTB20-siRNA + Ti group when

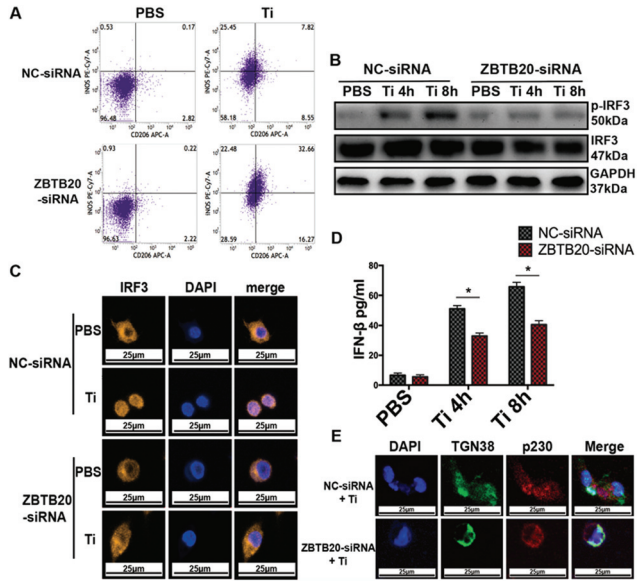

Fig. 6 ZBTB20 positively regulated TiPs-induced M1 polarization and stabilized p230 on the TGN. (A) ZBTB20 positively regulated TiPs-induced M1 polarization, but negatively regulated TiPs-induced M2 polarization (26.67 ± 1.57% iNOS-positive and 8.38 ± 0.93% CD206-positive in the NC-siRNA + Ti group; 21.35 ± 1.15% iNOS-positive and 11.95 ± 0.99% CD206-positive in the ZBTB20-siRNA + Ti group). (B) ZBTB20-siRNA reduced the TiPs-induced phosphorylation of IRF3 in BMDMs ($p < 0.05$). (C) ZBTB20-siRNA suppressed the TiPs-induced nuclear translocation of IRF3 (yellow) in BMDMs. (D) ZBTB20-siRNA resulted in lower cytokines production of IFN-β induced by TiPs ($p < 0.05$). (E) Binding of p230 (red) to TGN (green) was diminished in the ZBTB20-siRNA + Ti group when compared with that in the NC-siRNA + Ti group. *$p < 0.05$. Statistical significance was determined by means of a two-sided Student's *t*-test. All the data are shown as mean ± SD. The assays were performed at least three times for each sample.

compared with that in the NC-siRNA + Ti group (Fig. 6E). In brief, these data indicated that ZBTB20 positively regulated TiPs-induced M1 polarization and stabilized the localization of p230 on the TGN in BMDMs, which contributed toward cytokines secretion.

3.7 sh-ZBTB20 lentivirus injection reduced TiPs-induced osteolysis in C57BL/6J mouse calvaria

To investigate the role of ZBTB20 *in vivo*, we formulated a cranial osteolysis model with male C57BL/6J mice, as mentioned above, which were divided into six groups: (i) control (Control) group, (ii) TiPs (Ti) group, (iii) NC lentivirus + TiPs (NC + Ti) group, (iv) sh-ZBTB20 lentivirus + TiPs (sh-ZBTB20 + Ti) group, (v) mock lentivirus + TiPs (Mock + Ti) group, and (vi) ZBTB20-expressing lentivirus + TiPs ($ZBTB20^+$ + Ti) group; there were eight C57BL/6J mice in each group. Micro-CT data along with 3D reconstruction revealed that osteolysis was induced in the Ti group when compared with that in the Control group; TiPs-induced osteolysis was suppressed in the sh-ZBTB20 + Ti group when compared with the NC + Ti group, while TiPs-induced osteolysis was more exacerbated in the $ZBTB20^+$ + Ti group than that in the Mock + Ti group (Fig. 7A).

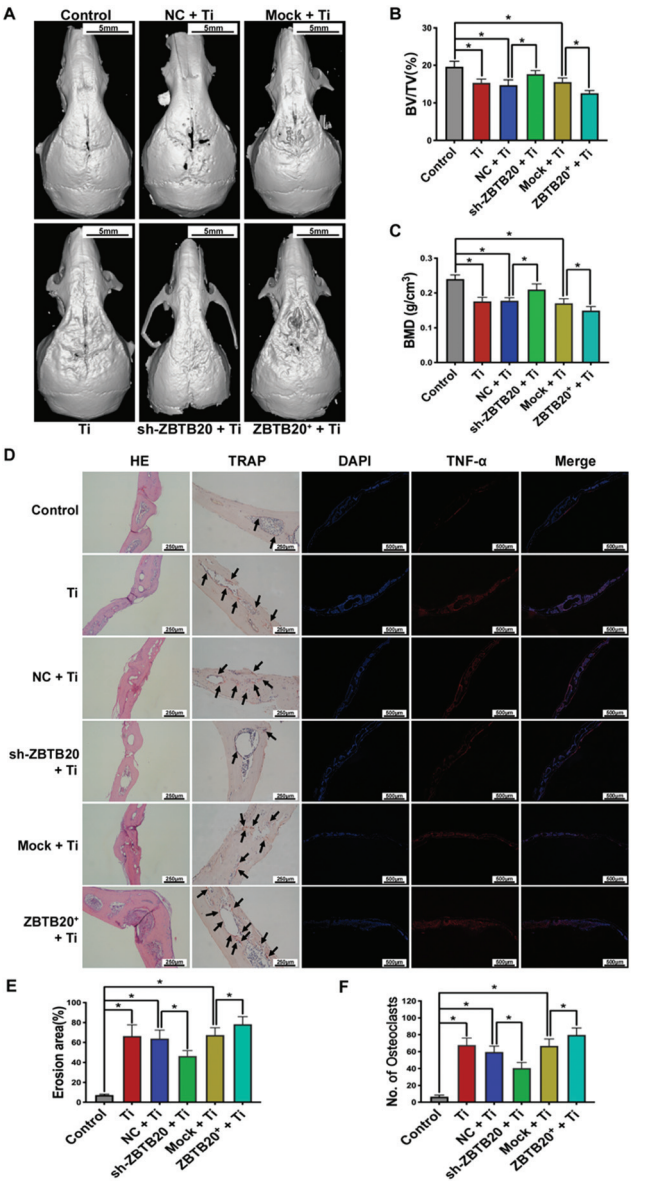

Fig. 7 sh-ZBTB20 lentivirus injection reduces TiPs-induced osteolysis and inflammation in C57BL/6J mouse calvaria. (A) Micro-CT showed that TiPs-induced osteolysis was suppressed in the sh-ZBTB20 + Ti group as compared to that in the NC + Ti group, and TiPs-induced osteolysis was exacerbated in the $ZBTB20^+$ + Ti group as compared to that in the Mock + Ti group. (B, C) Qualitative analysis of BV/TV and BMD data for Micro-CT-based 3D reconstructed images. (D) H&E staining, TRAP staining, and IF staining of C57BL/6J mouse calvaria. (E) Erosion area increased by 59.16 ± 12.7% ($p < 0.05$) in the Ti group as compared to that in the Control group, and it decreased by 17.38 ± 4.86% ($p < 0.05$) in the sh-ZBTB20 + Ti group when compared with that in the NC + Ti group. (F) Osteoclast numbers increased by 61.33 ± 11.17 ($p < 0.05$) in the Ti group when compared with that in the Control group, and they decreased by 19.17 ± 9.50 ($p < 0.05$) in the sh-ZBTB20 + Ti group when compared with those in the NC + Ti group. $n = 8$ for each group. *$p < 0.05$. Statistical significance was determined by one-way ANOVA with Fisher's LSD test. All the data are shown as mean ± SD. The assays were performed at least three times for each sample.

Moreover, we performed a qualitative analysis: the obtained BV/TV and BMD data are shown in Fig. 7B and C. We observed a decrease of 21.49 ± 3.35% ($p < 0.05$) in BV/TV and a decrease of 26.70 ± 5.58% ($p < 0.05$) in BMD in the Ti group when compared with those in the Control group; an increase of 19.19 ± 6.17% ($p < 0.05$) in BV/TV and an increase of 16.63 ± 11.53% ($p < 0.05$) in BMD in the sh-ZBTB20 + Ti group were observed when compared with those in the NC + Ti group; a decrease of 19.14 ± 4.58% ($p < 0.05$) in BV/TV and a decrease of 12.07 ± 9.09% ($p < 0.05$) in BMD were observed in the ZBTB20$^+$ + Ti group when compared with those in the Mock + Ti group. There were no statistical differences in the BV/TV and BMD data among the Ti, NC + Ti, and Mock + Ti groups.

To further assess the osteolysis and inflammation in the calvaria of C57BL/6J mice, H&E staining, TRAP staining, and IF staining were performed, as mentioned above. As shown in Fig. 7D–F, the erosion area increased by 59.16 ± 12.7% ($p < 0.05$) in the Ti group as compared to that in the Control group, decreased by 17.38 ± 4.86% ($p < 0.05$) in the sh-ZBTB20 + Ti group as compared to that in the NC + Ti group, and increased by 10.98 ± 8.43% ($p < 0.05$) in the ZBTB20$^+$ + Ti group as compared to that in the Mock + Ti group. With regard to TRAP staining, TRAP-positive osteoclast numbers increased by 61.33 ± 11.17 ($p < 0.05$) in the Ti group as compared to that in the Control group, decreased by 19.17 ± 9.50 ($p < 0.05$) in the sh-ZBTB20 + Ti group as compared to that in the NC + Ti group, and increased by 12.87 ± 10.35 ($p < 0.05$) in the ZBTB20$^+$ + Ti group as compared to that in the Mock + Ti group. There were no statistical differences in the erosion area and osteoclast numbers among the Ti, NC + Ti, and Mock + Ti groups. Consistently, the IF staining of TNF-α revealed that inflammation exacerbated in the Ti group when compared with that in the Control group, alleviated in the sh-ZBTB20 + Ti group as compared to that in the NC + Ti group, and exacerbated in the ZBTB20$^+$ + Ti group as compared to that in the Mock + Ti group. Similar trends were observed in the IHC staining of TNF-α and IL-6 (Fig. S7A†). Since CD206 is an M2 marker, we observed that due to the IF staining of CD206, the inflammation was exacerbated in the Ti group as compared to that in the Control group, was exacerbated in the sh-ZBTB20 + Ti group as compared to that in the NC + Ti group, and was alleviated in the ZBTB20$^+$ + Ti group as compared to that in the Mock + Ti group (Fig. S7B†). Due to the low expression of iNOS in the calvaria of C57BL/6J mice, we observed no differences with regard to the IF staining of iNOS among the six groups (Fig. S7C†). These findings suggested that TiPs-induced osteolysis and inflammation in the calvaria of C57BL/6J mouse was reduced by shZBTB20 lentivirus injection.

3.8 Effects of stably transfected RAW264.7 injection on TiPs-induced osteolysis in nude mice

In addition to the lentivirus injection on the calvaria of C57BL/6J mice, we built another cranial osteolysis model with RAW264.7 macrophage that was locally injected in nude mice, which were divided into seven groups: (i) bioluminescence (BLI) group, (ii) control (Control) group, (iii) TiPs (Ti) group, (iv) NC-RAW264.7 + TiPs (NC + Ti) group, (v) sh-ZBTB20-RAW264.7 + TiPs (sh-ZBTB20 + Ti) group, (vi) mock-RAW264.7 + TiPs (Mock + Ti) group, and (vii) ZBTB20-expressing-RAW264.7 + TiPs (ZBTB20$^+$ + Ti) group; there were eight nude mice in each group. The stably transfected RAW264.7 macrophages were locally injected as mentioned above. From day 0 to 7, the bioluminescence signals originating from the calvaria region could be clearly detected in the BLI group (Fig. 8A). Micro-CT-based 3D reconstructed images showed that osteolysis was induced in the Ti and BLI groups when compared with that in the Control group; TiPs-induced osteolysis was aggravated in the NC + Ti and Mock + Ti groups when compared with that in the Ti group. Meanwhile, TiPs-induced osteolysis was suppressed in the sh-ZBTB20 + Ti group when compared with that in the NC + Ti group, and TiPs-induced osteolysis was more exacerbated in the ZBTB20$^+$ + Ti group when compared with that in the Mock + Ti group (Fig. 8B). Qualitative analysis revealed that BV/TV decreased by 9.86 ± 8.68% ($p < 0.05$) and 12.07 ± 9.40% ($p < 0.05$) in the NC + Ti and Mock + Ti groups as compared to that in the Ti group, respectively, while the BMD values decreased by 15.13 ± 9.09% ($p < 0.05$) and 12.54 ± 10.91% ($p < 0.05$) in the NC + Ti and Mock + Ti groups as compared to that in the Ti group, respectively. Meanwhile, there was an increase of 14.33 ± 10.26% ($p < 0.05$) in BV/TV and an increase of 20.59 ± 7.70% ($p < 0.05$) in BMD in the sh-ZBTB20 + Ti group when compared with those in the NC + Ti group, as well as a decrease of 15.59 ± 10.90% ($p < 0.05$) in BV/TV and a decrease of 16.78 ± 4.01% ($p < 0.05$) in BMD in the ZBTB20$^+$ + Ti group when compared with those in the Mock + Ti group (Fig. 8C and D). In short, these data indicated that additional injections of local macrophages could aggravate TiPs-induced osteolysis, and ZBTB20-knockdown macrophages exerted a weakened osteolysis-promoting effect as compared to that by NC macrophages.

4. Discussion

In this study, we focused on elucidating that ZBTB20 positively regulated TiPs-induced macrophage-based inflammatory response and osteolysis, as well as investigating whether ZBTB20 could be utilized as a potential target to prevent AL. Emerging evidence suggests that AL is inseparable from the inflammatory reaction of macrophages.[14] Wear particles from prostheses, such as titanium and polymethylmethacrylate particles, can stimulate the macrophages to secrete proinflammatory cytokines.[15] These cytokines have been associated with the differentiation of macrophages into osteoclasts, activation of osteoclasts, and periprosthetic osteolysis.[16] In our recent study, we found that the targeted inhibition of TNF-α in macrophages could reduce osteolysis induced by TiPs,[17] which is consistent with the studies that have indicated the importance of proinflammatory cytokines in the bone microenvironment.[18] In our earlier report, we showed that PRRs (*e.g.*, TLR4 and NOD2) played important roles in the activation of macrophages by TiPs.[10,12] Another study showed that NF-κB

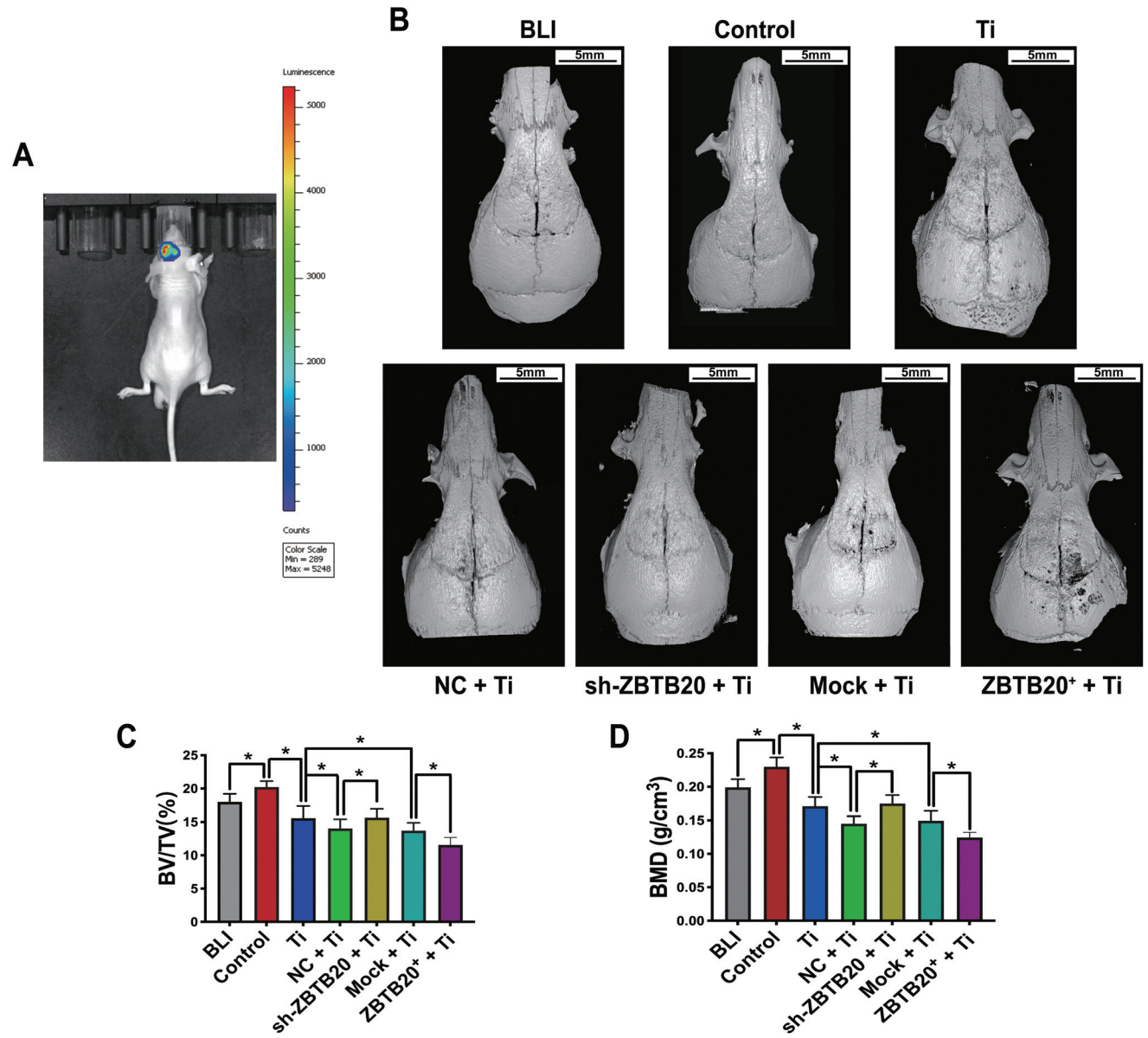

Fig. 8 Effects of RAW264.7 injection on TiPs-induced osteolysis in nude mice. (A) BLI signals could be observed in the calvaria region of nude mice. (B) Micro-CT-based 3D reconstructed images reveal that osteolysis was induced in the Ti and BLI groups when compared with that in the Control group; TiPs-induced osteolysis was aggravated in the NC + Ti and Mock + Ti groups when compared with that in the Ti group; TiPs-induced osteolysis was suppressed in the sh-ZBTB20 + Ti group when compared with that in the NC + Ti group; and TiPs-induced osteolysis was more exacerbated in the ZBTB20^{+} + Ti group when compared with that in the Mock + Ti group. (C and D) Qualitative analyses of BV/TV and BMD. n = 8 for each group. *p < 0.05. Statistical significance was determined by one-way ANOVA along with Fisher's LSD test. All the data are shown as mean ± SD. The assays were performed at least three times for each sample.

and MAPK are two pivotal signaling pathways using which proinflammatory responses are upregulated.[19] These results suggest that TiPs activated the BMDMs and induced the production of proinflammatory cytokines *via* the NF-κB signaling pathway and IRF3 phosphorylation.

The mechanism by which wear particles activate macrophages is not fully understood. Some high-throughput sequencing work on AL is necessary, which is still lacking in various databases. Therefore, we generated the mRNA profiles of RAW264.7 macrophages pretreated with TiPs. Our current study indicated that targeting ZBTB20 could inhibit the inflammatory reaction of macrophages, which would benefit the prevention and treatment of AL.[20] ZBTB20 is currently recognized as a regulator of gene expression; consequently, it plays critical roles in a wide array of biological processes, such as inflammation, metabolism, proliferation, and cell differentiation.[21,22] In the current study, we have demonstrated that the protein expression of ZBTB20 in the AL group was significantly higher than that in the FHN group. Based on the knockdown/overexpression of ZBTB20, we further clarified that

ZBTB20 positively regulates TiPs-induced inflammatory responses in BMDMs, which suggests that ZBTB20 could participate in the occurrence and development of AL.

Some recent reports have suggested that ZBTB20 can regulate the NF-κB signaling pathway as a regulator of IκBα.[8,23] The expression of ZBTB20 in BMDMs was found to be upregulated after the stimulation of LPS, and the promoter sequence of the *IκBα* gene was found to bind to the ZBTB20 protein, which repressed *IκBα* gene transcription.[8] Another study showed that the expression of IκBα protein increased by knocking down the *Zbtb20* gene, thereby inhibiting NF-κB activation as well as cell migration and invasion of gastric cancer.[23] Our earlier reports have shown that the forced overexpression of SHP reduced the TiPs-induced osteolysis effect by downregulating the expression of IKKγ and inhibiting NF-κB activation.[10] We also investigated triptolide, an active compound of the medicinal herb *Tripterygium wilfordii Hook F*, which could suppress RANKL-mediated NF-κB activation and TiPs-induced osteolysis.[24] In the current study, we confirmed that the knockdown of ZBTB20 reduced NF-κB activation induced by TiPs by binding the promoter of the *IκBα* gene and repressing *IκBα* gene transcription; interestingly enough, the knockdown of IκBα rescued the antiinflammatory effect caused by ZBTB20 knockdown in BMDMs, which suggested that the downregulation of ZBTB20 by novel approaches could be a therapeutic approach for the treatment of AL with better outcomes.

Emerging evidence suggests that the processes of AL are linked with macrophage polarization, as reviewed recently,[11,25] which is also consistent with our recent studies on NOD2 receptors.[12] Some proinflammatory cytokines, such as TNF-α, lead to the activation of M1-related genes.[26] Since ZBTB20 functioned as a positive regulator of TNF-α in the current study, the knockdown of ZBTB20 may reduce the differentiation of M1 macrophages and promote the differentiation of M2 macrophages, which was validated by our flow cytometry analysis. Moreover, in contrast to other studies,[8] we showed that the knockdown of ZBTB20 attenuated the activation of IRF3 and the production of IFN-β cytokines. This discrepancy might be due to the different types of stimuli, as well as the duration and concentration of stimuli. A number of studies have shown that the final secretion of proinflammatory factors depends on the TGN-derived tubular carriers, which transfer cytokines to the cell surface for release; further, p230 was identified as a crucial marker of TGN-derived tubular carriers.[27,28] In the current study, we reported that the knockdown of ZBTB20 stabilized the localization of p230 on TGN and inhibited the production of tubular carriers in BMDMs. Therefore, targeting the ZBTB20 of macrophages is expected to provide a novel approach for the treatment of AL *via* reducing M1 differentiation as well as producing and secreting proinflammatory factors.

To this end, we reported earlier that a local injection of NOD2-knockdown lentivirus exacerbated TiPs-induced osteolysis in mouse crania,[12] suggesting that a local lentivirus injection may be a novel method for the treatment of AL by targeting multiple regulatory genes. This is also consistent with reports documenting that a local injection of adeno-associated virus (AAV) could improve the treatment of some debilitating diseases, such as rheumatoid arthritis and amyotrophic lateral sclerosis.[29,30] In this work, we locally injected ZBTB20-knockdown lentivirus and ZBTB20-expressing lentivirus on mouse crania: the obtained results suggest that ZBTB20-knockdown lentivirus reduced TiPs-induced osteolysis. Moreover, the distribution of lentivirus could not be observed and quantified after the injection. Therefore, according to our earlier work and other studies,[31] we formulated another cranial osteolysis model with a local injection of RAW264.7 macrophage in nude mouse crania; consequently, the bioluminescence signals originating from the calvaria region could be clearly detected. From these results, we conclude that the knockdown of ZBTB20 leads to the upregulation of IκBα and inhibition of TiPs-induced NF-κB activation in BMDMs; these are consistent with the decreased expressions of proinflammatory factors, inhibited cytokine secretions, and reduced M1 differentiation. Most interestingly, TiPs-induced osteolysis on mouse crania could be attenuated by ZBTB20-knockdown lentivirus injection, further suggesting that ZBTB20 may mediate wear-particle-induced peri-implant osteolysis; therefore, ZBTB20 could be a potential therapeutic target for AL with better treatment outcomes in the future.

5. Conclusion

In conclusion, our results highlight the importance of ZBTB20 as a positive regulator of TiPs-induced osteolysis. We performed RNA-Seq transcriptome analysis of RAW264.7 macrophages; the obtained results showed that ZBTB20 could be a vital target in macrophage activation and TiPs-induced osteolysis. By constructing shRNA and overexpression lentivirus, we observed that ZBTB20 regulated the TiPs-induced inflammatory reaction of macrophages by adjusting the NF-kB pathway and polarization. Then, we performed *in vivo* studies using local lentivirus injection, local macrophage injection, and bioluminescence to reveal the effects of ZBTB20 on TiPs-induced cranial osteolysis. Taken together, the results of this study may provide a new strategy for AL therapy. We are currently expanding this concept to other potential target genes. On other research fronts, a comprehensive study of biological pathways and mechanisms are necessary to establish a clear functional relationship between the local lentivirus injection and alleviated TiPs-induced cranial osteolysis.

Conflicts of interest

The authors declare no conflict of interest.

Acknowledgements

This work was supported by the National Natural Science Foundation of China (81672186) and Natural Science

Foundation of Guangdong Province Key Project (2017B030311016).

References

1 M. Wang and T. Tang, Surface treatment strategies to combat implant-related infection from the beginning, *J. Orthop. Translat.*, 2019, **17**, 42–54.
2 J. J. Yao, H. Maradit Kremers, M. P. Abdel, D. R. Larson, J. E. Ransom, D. J. Berry and D. G. Lewallen, Long-term Mortality After Revision THA, *Clin. Orthop. Relat. Res.*, 2018, **476**(2), 420–426.
3 S. B. Goodman and J. Gallo, Periprosthetic Osteolysis: Mechanisms, Prevention and Treatment, *J. Clin. Med.*, 2019, **8**(12), pii: E2091.
4 H. Shao, J. Shen, M. Wang, J. Cui, Y. Wang, S. Zhu, W. Zhang, H. Yang, Y. Xu and D. Geng, Icariin protects against titanium particle-induced osteolysis and inflammatory response in a mouse calvarial model, *Biomaterials*, 2015, **60**, 92–99.
5 M. Nagao, T. Ogata, Y. Sawada, and Y. Gotoh, Zbtb20 promotes astrocytogenesis during neocortical development, *Nat. Commun.*, 2016, **7**, 11102.
6 Y. Zhang, Z. Xie, L. Zhou, L. Li, H. Zhang, G. Zhou, X. Ma, P. L. Herrera, Z. Liu, M. J. Grusby and W. J. Zhang, The zinc finger protein ZBTB20 regulates transcription of fructose-1,6-bisphosphatase 1 and beta cell function in mice, *Gastroenterology*, 2012, **142**(7), 1571–1580.e6.
7 G. Liu, L. Zhou, H. Zhang, R. Chen, Y. Zhang, L. Li, J. Y. Lu, H. Jiang, D. Liu, S. Qi, Y. M. Jiang, K. Yin, Z. Xie, Y. Shi, Y. Liu, X. Cao, Y. X. Chen, D. Zou, and W. J. Zhang, Regulation of hepatic lipogenesis by the zinc finger protein Zbtb20, *Nat. Commun.*, 2017, **8**, 14824.
8 X. Liu, P. Zhang, Y. Bao, Y. Han, Y. Wang, Q. Zhang, Z. Zhan, J. Meng, Y. Li, N. Li, W. J. Zhang and X. Cao, Zinc finger protein ZBTB20 promotes Toll-like receptor-triggered innate immune responses by repressing IkappaBalpha gene transcription, *Proc. Natl. Acad. Sci. U. S. A.*, 2013, **110**(27), 11097–11102.
9 Z. Yan, S. Zhu, H. Wang, L. Wang, T. Du, Z. Ye, D. Zhai, Z. Zhu, X. Tian, Z. Lu and X. Cao, MOTS-c inhibits Osteolysis in the Mouse Calvaria by affecting osteocyte-osteoclast crosstalk and inhibiting inflammation, *Pharmacol. Res.*, 2019, **147**, 104381.
10 C. Zhang, C. Li, S. Li, L. Qin, M. Luo, G. Fu, J. Qiu, P. Peng, W. Cai and Y. Ding, Small Heterodimer Partner Negatively Regulates TLR4 Signaling Pathway of Titanium Particles-Induced Osteolysis in Mice, *J. Biomed. Nanotechnol.*, 2018, **14**(3), 609–618.
11 S. B. Goodman, E. Gibon, J. Pajarinen, T. H. Lin, M. Keeney, P. G. Ren, C. Nich, Z. Yao, K. Egashira, F. Yang and Y. T. Konttinen, Novel biological strategies for treatment of wear particle-induced periprosthetic osteolysis of orthopaedic implants for joint replacement, *J. R. Soc., Interface*, 2014, **11**(93), 20130962.
12 S. Li, J. Qiu, L. Qin, P. Peng, C. Li, J. Mao, G. Fang, Z. Chen, S. Lin, Y. Fu, W. Cai and Y. Ding, NOD2 negatively regulated titanium particle-induced osteolysis in mice, *Biomater. Sci.*, 2019, **7**(7), 2702–2715.
13 G. Fu, S. Li, N. Ouyang, J. Wu, C. Li, W. Liu, J. Qiu, P. Peng, L. Qin and Y. Ding, Antiresorptive Agents are More Effective in Preventing Titanium Particle-Induced Calvarial Osteolysis in Ovariectomized Mice Than Anabolic Agents in Short-Term Administration, *Artif. Organs*, 2018, **42**(9), E259–E271.
14 N. A. Athanasou, The pathobiology and pathology of aseptic implant failure, *Bone Joint Res.*, 2016, **5**(5), 162–168.
15 C. P. Rader, T. Sterner, F. Jakob, N. Schutze and J. Eulert, Cytokine response of human macrophage-like cells after contact with polyethylene and pure titanium particles, *J. Arthroplasty*, 1999, **14**(7), 840–848.
16 S. B. Goodman, T. Ma, R. Chiu, R. Ramachandran and R. L. Smith, Effects of orthopaedic wear particles on osteoprogenitor cells, *Biomaterials*, 2006, **27**(36), 6096–6101.
17 C. Q. Qin, Y. Ding, D. S. Huang, J. Xu, R. F. Ma and J. B. Huang, Down-regulation of TNF-alpha by small interfering RNA inhibits particle-induced inflammation in vitro, *Artif. Organs*, 2011, **35**(7), 706–714.
18 J. Kzhyshkowska, A. Gudima, V. Riabov, C. Dollinger, P. Lavalle and N. E. Vrana, Macrophage responses to implants: prospects for personalized medicine, *J. Leukocyte Biol.*, 2015, **98**(6), 953–962.
19 J. He, J. Li, H. Liu, Z. Yang, F. Zhou, T. Wei, Y. Dong, H. Xue, L. Tang and M. Liu, Scandoside Exerts Anti-Inflammatory Effect Via Suppressing NF-kappaB and MAPK Signaling Pathways in LPS-Induced RAW 264.7 Macrophages, *Int. J. Mol. Sci.*, 2018, **19**(2), 457.
20 J. X. Wang, L. F. Hou, Y. Yang, W. Tang, Y. Li and J. P. Zuo, SM905, an artemisinin derivative, inhibited NO and pro-inflammatory cytokine production by suppressing MAPK and NF-kappaB pathways in RAW 264.7 macrophages, *Acta Pharmacol. Sin.*, 2009, **30**(10), 1428–1435.
21 C. Zhu, G. Chen, Y. Zhao, X. M. Gao and J. Wang, Regulation of the Development and Function of B Cells by ZBTB Transcription Factors, *Front. Immunol.*, 2018, **9**, 580.
22 T. R. Doeppner, J. Herz, M. Bahr, A. B. Tonchev and A. Stoykova, Zbtb20 Regulates Developmental Neurogenesis in the Olfactory Bulb and Gliogenesis After Adult Brain Injury, *Mol. Neurobiol.*, 2019, **56**(1), 567–582.
23 Y. Zhang, X. Zhou, M. Zhang, L. Cheng, Y. Zhang and X. Wang, ZBTB20 promotes cell migration and invasion of gastric cancer by inhibiting IkappaBalpha to induce NF-kappaB activation, *Artif. Cells, Nanomed., Biotechnol.*, 2019, **47**(1), 3862–3872.
24 J. Huang, L. Zhou, H. Wu, N. Pavlos, S. M. Chim, Q. Liu, J. Zhao, W. Xue, R. X. Tan, J. Ye, J. Xu, E. S. Ang, H. Feng, J. Tickner, J. Xu and Y. Ding, Triptolide inhibits osteoclast formation, bone resorption, RANKL-mediated NF-B activation and titanium particle-induced osteolysis in a mouse model, *Mol. Cell. Endocrinol.*, 2015, **399**, 346–353.

25 A. J. Rao, E. Gibon, T. Ma, Z. Yao, R. L. Smith and S. B. Goodman, Revision joint replacement, wear particles, and macrophage polarization, *Acta Biomater.*, 2012, **8**(7), 2815–2823.

26 M. Sun, Z. Deng, F. Shi, Z. Zhou, C. Jiang, Z. Xu, X. Cui, W. Li, Y. Jing, B. Han, W. Zhang and S. Xia, Rebamipide-loaded chitosan nanoparticles accelerate prostatic wound healing by inhibiting M1 macrophage-mediated inflammation via the NF-kappaB signaling pathway, *Biomater. Sci.*, 2020, **8**(3), 912–925.

27 M. Micaroni, A. C. Stanley, T. Khromykh, J. Venturato, C. X. Wong, J. P. Lim, B. J. Marsh, B. Storrie, P. A. Gleeson and J. L. Stow, Rab6a/a' are important Golgi regulators of pro-inflammatory TNF secretion in macrophages, *PLoS One*, 2013, **8**(2), e57034.

28 Z. Z. Lieu, J. G. Lock, L. A. Hammond, N. L. La Gruta, J. L. Stow and P. A. Gleeson, A trans-Golgi network golgin is required for the regulated secretion of TNF in activated macrophages in vivo, *Proc. Natl. Acad. Sci. U. S. A.*, 2008, **105**(9), 3351–3356.

29 M. Bravo-Hernandez, T. Tadokoro, M. R. Navarro, O. Platoshyn, Y. Kobayashi, S. Marsala, A. Miyanohara, S. Juhas, J. Juhasova, H. Skalnikova, Z. Tomori, I. Vanicky, H. Studenovska, V. Proks, P. Chen, N. Govea-Perez, D. Ditsworth, J. D. Ciacci, S. Gao, W. Zhu, E. T. Ahrens, S. P. Driscoll, T. D. Glenn, M. McAlonis-Downes, S. Da Cruz, S. L. Pfaff, B. K. Kaspar, D. W. Cleveland and M. Marsala, Spinal subpial delivery of AAV9 enables widespread gene silencing and blocks motoneuron degeneration in ALS, *Nat. Med.*, 2020, **26**(1), 118–130.

30 C. H. Evans, S. C. Ghivizzani and P. D. Robbins, Gene Delivery to Joints by Intra-Articular Injection, *Hum. Gene Ther.*, 2018, **29**(1), 2–14.

31 A. Nabeshima, J. Pajarinen, T. H. Lin, X. Jiang, E. Gibon, L. A. Cordova, F. Loi, L. Lu, E. Jamsen, K. Egashira, F. Yang, Z. Yao and S. B. Goodman, Mutant CCL2 protein coating mitigates wear particle-induced bone loss in a murine continuous polyethylene infusion model, *Biomaterials*, 2017, **117**, 1–9.